

DISSERTATION

INFLUENCE OF CARDIOLIPIN REMODELING ON MITOCHONDRIAL RESPIRATORY
FUNCTION IN THE HEART

Submitted by

Catherine Hoang Le

Graduate Degree Program in Cell and Molecular Biology

In partial fulfillment of requirements

For the Degree of Doctor of Philosophy

Colorado State University

Fort Collins, Colorado

Summer 2013

Doctoral Committee:

Advisor: Adam J. Chicco

Gerrit J. Bouma

Karyn L. Hamilton

Michael J. Pagliassotti

ABSTRACT

INFLUENCE OF CARDIOLIPIN REMODELING ON MITOCHONDRIAL RESPIRATORY FUNCTION IN THE HEART

The following investigation comprises a series of experiments with the overall aim of elucidating the role of cardiolipin acyl-chain remodeling on mitochondrial respiratory function in the mammalian heart. The experiments tested the general hypothesis that changes in the fatty acid composition of cardiolipin, a unique mitochondrial phospholipid, contribute to cardiac mitochondrial respiratory dysfunction, which is believed to be an underlying mechanism of myocardial hypertrophy and contractile dysfunction in several cardiac pathologies. The specific aims of each experimental series were to: 1) Determine the influence of cardiolipin compositional changes on cardiac mitochondrial respiratory function in models of aging, pressure overload hypertrophy and heart failure, and 2) Determine how defects in the cardiolipin remodeling process itself elicits cardiac mitochondrial respiratory dysfunction associated with a genetic childhood-onset cardiomyopathy, known as Barth syndrome. Studies in Aim 1 demonstrated that the distinct pattern of aberrant cardiolipin remodeling observed in the aged and failing heart resulted from increased metabolism of polyunsaturated fatty acids (PUFAs), which predominate in the cardiolipin molecular species. Pharmacological inhibition of delta-6 desaturase, the rate-limiting enzyme in the PUFA metabolism pathway, reversed cardiolipin remodeling, reduced myocardial hypertrophy and preserved contractile function in the rodent models of aging, pressure overload and hypertensive heart disease. However, in contrast to our hypothesis, reversal of these changes in cardiolipin composition did not have a significant effect on mitochondrial respiratory function, dissociating alterations in cardiolipin composition from

cardiac mitochondrial respiratory dysfunction in these conditions. Studies in Aim 2 demonstrated a marked substrate-specific impairment of cardiac mitochondrial respiratory function in mice lacking the cardiolipin remodeling enzyme, tafazzin. Cardiac mitochondria from tafazzin-deficient mice demonstrated a selective impairment in carbohydrate and lipid oxidation and a dramatic decrease in pantothenic acid amounts. These data suggest a role of tafazzin in the transport, activation, and/or generation of reducing equivalents by the TCA cycle. Additionally, these data implicate impairment of tafazzin function and/or cardiolipin remodeling process itself, rather than alter cardiolipin composition *per se*, in mitochondrial dysfunction associated in Barth syndrome. Collectively, these findings challenge previous studies suggesting that alterations of the distinctly uniform acyl-chain composition of cardiolipin impair cardiac mitochondrial respiration. Rather, they instead show that the widely observed redistribution of cardiolipin PUFA content in chronic cardiac pathologies appears to reflect a global increase in PUFA metabolism that profoundly influences cardiac structure and function by mechanisms we are only beginning to understand. Interestingly, the cardiolipin remodeling process itself and/or tafazzin enzyme may play a more important role than previously thought in cardiac mitochondrial respiratory function and cardiomyopathy.

ACKNOWLEDGMENTS

The authors would like to thank Allen Medway and Dr. Brian Stauffer for assistance with obtaining human heart samples and patient information at the University of Colorado Denver, Juliano Silveria for assistance with the qRT-PCR, Carolyn Broccardo for assistance with the proteomic analyses, and Victoria Harcy for assistance with maintenance of the *Taz* shRNA mouse colony. All work was funded by a Scientist Development Grant from the American Heart Association (0835545N), Barth Syndrome Foundation grant, and a NIH award HL094890-01A1 (A.J.C.).

TABLE OF CONTENTS

ABSTRACT	ii-iii
ACKNOWLEDGEMENTS	iv
TABLE OF CONTENTS	v-vi
CHAPTER 1-INTRODUCTION AND EXPERIMENTAL AIMS	1-4
CHAPTER II-“Inhibition of delta-6-desaturase reverses cardioplipin remodeling and prevents contractile dysfunction in the aged mouse heart without altering mitochondrial respiratory function”	5
Summary	5-6
Introduction.....	6-7
Experimental Procedures	7-12
Results.....	12-14
Discussion.....	15-18
Tables 2.1-2.3	19-22
Figures 2.1-2.5	23-27
CHAPTER III-“Delta-6-desaturase links PUFA metabolism with phospholipid remodeling and disease progression in heart failure”	28
Summary	28-29
Introduction.....	29-31
Experimental Procedures	31-35
Results.....	35-39
Discussion.....	39-43
Table 3.1	44

Figures 3.1-3.7	45-51
CHAPTER IV-“Substrate-specific impairment of oxidative phosphorylation in <i>Taz</i> -deficient cardiac mitochondria”	52
Summary	52-53
Introduction.....	53-55
Experimental Procedures	55-62
Results.....	63-65
Discussion	65-70
Tables 4.1-4.2	71-73
Figures 4.1-4.4	74-77
CHAPTER V-OVERALL CONCLUSIONS	78-79
REFERENCES	80-89

CHAPTER 1-INTRODUCTION AND EXPERIMENTAL AIMS

Cardiolipin (CL) is a unique tetra-acyl phospholipid located in the inner mitochondrial membrane where it is required for the structural integrity of the mitochondria and for the proper function of membrane proteins involved in oxidative phosphorylation. In the healthy mammalian heart, the essential polyunsaturated fatty acid (PUFA) linoleic acid (LA; 18:2n6) makes up 80-90% of CL acyl chains, and tetra-linoleoyl CL (18:2₄ CL) accounts for approximately 77-80% of the total CL pool. This distinct compositional uniformity is highly conserved across mammalian species, and has therefore been hypothesized to be important for the structural and/or functional support cardiolipin provides to mitochondrial membrane proteins. Reduction of 18:2₄ CL has been associated with mitochondrial respiratory dysfunction and increased ROS production in animal models of cardiac pathology such as heart failure, diabetic cardiomyopathy, aging, and ischemia. However, a causal link between altered cardiolipin composition and cardiac mitochondrial dysfunction has remained unclear due to the absence of experimental studies that selectively target the incompletely understood mechanisms of aberrant cardiolipin remodeling in the mammalian heart.

Despite distinct etiologies and genetic backgrounds, the pattern of aberrant CL remodeling in cardiac pathologies has consistently manifested as a marked decrease in linoleic acid with corresponding increases in long-chain highly unsaturated fatty acids (HUFAs) such as arachidonic acid (AA; 20:4n6) and/or docosahexaenoic acid (DHA; 22:6n-3). While several hypotheses have been explored, the mechanisms and pathophysiological relevance of this remodeling pattern have remained unclear. In the absence of dietary supplementation, desaturation and elongation of LA and ALA (alpha-linolenic acid; 18:3n3) provide the majority

of long-chain PUFAs present in mammalian tissues. Delta-6 desaturase (D6D) is a microsomal enzyme that catalyzes the rate-limiting step in the pathway of n-3 and n-6 synthesis of the HUFAs, AA and DHA from their dietary precursors, LA and ALA, respectively. However, the potential influence of PUFA metabolism by the D6D pathway on cardiolipin composition has not been previously examined. Rather, attention was placed on defining the critical enzyme-catalyzed steps involved in the cardiolipin acyl chain remodeling process itself, which has recently established a central role of a phospholipid transacylase known as tafazzin (*Taz*).

Tafazzin is a phospholipid transacylase known to be responsible for the acyl chain remodeling of cardiolipin following *de novo* biosynthesis in mitochondria despite having no acyl specificity itself. Tafazzin functions to transfer acyl residues from adjacent phospholipids to lysophospholipids. Mutations in tafazzin result in CL deficiency with a marked loss of LA enrichment, an accumulation of monolyso-CL, and a progressive cardioskeletal myopathy phenotype in the X-linked genetic disorder known as Barth Syndrome (BTHS). The resulting depletion of tetra-linoleoyl CL is the molecular signature of BTHS, which is characterized by childhood-onset dilated cardiomyopathy, exercise intolerance, chronic fatigue, delayed growth, and neutropenia. The existence of this severe phenotype suggests a critical biological role of CL remodeling in human health and is highly suggestive of mitochondrial dysfunction as a central mechanism of BTHS. Indeed, *Taz* mutations have been associated with decreased mitochondrial respiratory enzyme function, increased production of reactive oxygen species (ROS), and/or impaired mitochondrial protein sorting and import in BTHS cell lines, *Taz*-deficient yeast, *Drosophila*, and zebrafish models. While these studies have been valuable in elucidating the cellular and/or molecular consequences of tafazzin deficiency, until recently, there was no means of assessing the influence of tafazzin deficiency on mammalian cardiac mitochondrial function.

This body of work collectively tests two specific hypotheses aimed at elucidating the role of cardiolipin remodeling on cardiac mitochondrial dysfunction associated with aging, heart failure, and BTHS.

Overall hypothesis: Enrichment of cardiolipin with linoleic acid has an important biological role in maintaining optimal cardiac mitochondrial respiratory function. Decreases in the linoleic acid content of CL associated with aging, heart failure and BTHS lead to cardiac mitochondrial respiratory dysfunction, thereby contributing to impaired cardiac function associated with these conditions.

Specific Aims

Specific Aim 1: Determine whether the loss of linoleic acid and corresponding increases in long-chain PUFAs in cardiolipin contributes to the cardiac mitochondrial respiratory dysfunction associated with aging and heart failure.

Aim 1.1: Determine whether reversing this pattern of cardiolipin remodeling by *in vivo* inhibition of delta-6 desaturase resolves cardiac mitochondrial respiratory dysfunction in aged C57Bl/6 mice.

Aim 1.2: Determine whether reversing this pattern of cardiolipin remodeling by *in vivo* inhibition of delta-6 desaturase preserves mitochondrial respiratory function in the pressure overloaded and failing hypertensive rat heart.

Specific Aim 2: Characterize the cardiac mitochondrial respiratory phenotype of *Taz*-deficient (*Taz*-shRNA) mice to elucidate how impairment of the cardiolipin remodeling process itself influences cardiac mitochondrial respiratory function.

Inhibition of delta-6-desaturase reverses cardiolipin remodeling and prevents contractile dysfunction in the aged mouse heart without altering mitochondrial respiratory function¹

Summary

Alterations in the fatty acid composition of cardiolipin (CL), a mitochondrial phospholipid, may contribute to mitochondrial dysfunction associated with myocardial aging, but its mechanism and role in this process remains unclear. We hypothesized that CL remodeling in the aged heart, characterized by a loss of linoleic acid (LA) and increase in highly unsaturated fatty acids (HUFAs), results from increased activity of delta 6-desaturase (D6D), which catalyzes the production of HUFAs from essential fatty acids such as LA. Aged (24 mo) C57Bl/6 mice were administered a selective D6D inhibitor (SC-26196, 100 mg/kg/d; SC) or no drug for 4 weeks, followed by isolation of cardiac subsarcolemmal (SSM) and interfibrillar (IFM) mitochondria for assessment of respiratory function and CL composition. Aged hearts exhibited a classic pattern of CL remodeling in IFM, but not SSM, which paralleled a 25% loss in state 3 respiration in IFM only. SC reversed CL remodeling in IFM, but had no effect on mitochondrial respiration. Interestingly, SC also reduced heart weight, reversed left ventricular dilation and attenuated contractile dysfunction in aged mice. These studies indicate that D6D plays a pivotal

¹ Catherine H. Le^{*}, Christopher M. Mulligan⁺, Anthony B. deMooy[#],
Christopher B. Nelson^{*}, Adam J. Chicco, PhD^{*+##†}

Integrative Cardiac Biology Laboratory, Departments of ^{*}Program in Cell and Molecular Biology, ⁺Food Science and Human Nutrition, [#]Biomedical Sciences, and [†]Health and Exercise Science, Colorado State University, Fort Collins, CO 80523-1582

role in CL remodeling in the aged heart, but argue against the role of this process in mitochondrial dysfunction. However, the mechanism by which D6D influences remodeling and function of the senescent heart warrants further investigation.

Introduction

Aging is associated with progressive cardiac hypertrophy and contractile impairment and is a primary risk factor for heart failure in humans [1, 2]. Deterioration of cardiac mitochondrial function, manifesting as impaired bioenergetics and/or increased production of reactive oxygen species (ROS), have been thought to be a primary contributor to myocardial aging and associated pathologies [3-5]. However, the extent, mechanisms and pathophysiological importance of mitochondrial dysfunction in cardiac aging remain controversial.

The fatty acid composition of cardiac membrane phospholipids changes with advancing age [6-9] and is highly predictive of maximal lifespan across mammalian species [10-12]. Remodeling of phospholipids may be particularly relevant in mitochondrial membranes, where it has been suggested as a central mechanism of age-associated mitochondrial dysfunction and oxidative stress [8, 13-15]. Interestingly, across several experimental models and species, the predominant compositional change in cardiac phospholipids is a proportional loss of the essential polyunsaturated fatty acid (PUFA) linoleic acid (18:2n6; LA), matched by increases in the long chain highly unsaturated fatty acids arachidonic acid (20:4n6; AA) and/or docosahexaenoic acid (22:6n3; DHA). This observed increase in PUFA metabolism may involve delta-6-desaturase (D6D), the rate-limiting enzyme in PUFA biosynthesis. This pattern of remodeling is particularly important with regard to the mitochondrial phospholipid cardiolipin, which is normally highly enriched with LA and plays a key role in maintaining the structural integrity of mitochondrial

proteins and supporting optimal mitochondrial function [15]. Accumulation of AA and DHA in phospholipids increases the membrane's susceptibility to peroxidative damage by ROS, which may further contribute the aging process by increasing the accumulation of lipid peroxidation by-products and/or impairing membrane-dependent processes [11]. However, determining the extent to which compositional changes in cardiolipin or other mitochondrial phospholipids contribute to age-related mitochondrial dysfunction has remained unclear due to the absence of experimental studies demonstrating reversal of the process in an aging model.

In the present study, we hypothesized that the loss of LA with corresponding increases in AA and DHA in the aged heart contributes to cardiac mitochondrial respiratory function. Additionally, we tested that inhibition of D6D will reverse age-related changes in cardiolipin composition by preserving myocardial LA bioavailability and reducing endogenous biosynthesis of AA and DHA. Young and senescent C57Bl/6 mice were treated with an orally active selective D6D inhibitor or no drug for 4 weeks, followed by examination of cardiac mitochondrial phospholipid composition, respiratory function, ROS release and lipid peroxidation, along with assessment of myocardial structure and function. Our studies reveal a pivotal effect of essential PUFA metabolism on cardiolipin composition, hypertrophy and contractile function in the aged heart, but dissociate these phenomena from changes in cardiac mitochondrial respiratory function, ROS release, and lipid peroxidation.

Experimental Procedures

Animal model of cardiac aging

To determine the nature and extent of cardiolipin remodeling in the C57Bl/6 mouse model of aging, heart tissues were obtained from 4 month and 24 month old mice (n = 4 /group)

from the National Institutes on Aging (NIA) tissue bank for assessment of phospholipid fatty acid composition. Following confirmation of the signature remodeling pattern reported in aged rats [8] and humans with heart failure [16] (Table S1), male C57BL/6 mice were obtained from the NIA aging colony at 4 months (young; n = 12) and 24 months (Old; n = 12) of age for experimental studies. All mice were maintained on standard chow *ad libitum* (Harlan Teklad 2918) for 4 weeks prior to being randomly assigned to D6D inhibition or control groups (n = 6/group).

Inhibition of D6D in vivo

To chronically inhibit systemic D6D activity *in vivo*, mice were administered the potent, orally active D6D inhibitor SC-26196 (Biofine, Inc., Blaine, WA), at a dose previously reported to selectively inhibit D6D enzyme activity with no effect on other desaturase enzymes in mice *in vivo* (100 mg/kg/d mixed in chow) for 4-weeks based on daily food consumption records taken over 3-4 weeks prior to treatment [17]. Following the 4-week experimental period, animals were deeply anesthetized with 100 mg/kg sodium pentobarbital and sacrificed by midline thoracotomy and removal of the heart. All procedures were approved by the Colorado State University Care and Use Committee and conform to the *Guide for the Care and Use of Laboratory Animals* published by the U.S. National Institutes of Health (NIH Publication No. 85-23, revised 1996).

Mitochondrial isolation

Mitochondria were freshly isolated from ~100mg of heart tissue in cold Chappell-Perry buffer consisting of (in mM) KCl (100), MOPS (50), EGTA (1), EGTA (5), MgSO₄·7H₂O (5), and ATP (1), pH 7.4 (with KOH) by standard differential centrifugation methods as previously

described with minor modifications [16]. To determine if aging or D6D activity differentially affects the two spatially distinct mitochondrial subpopulations present in cardiomyocytes, both subsarcolemmal (SSM) and intermyofibrillar (IFM) mitochondria were isolated, using trypsin to dissociate IFM from myofibrillar proteins.

Fatty acid composition of tissue and mitochondrial phospholipids

Lipids were extracted from heart tissue (~20mg) or serum (50 μ L) by incubation in 800 μ L methanol with 25 μ L sodium methoxide solution to generate phospholipid fatty acid methyl esters, followed by extraction of fatty acids with hexane for assessment of total phospholipid fatty acid composition by gas chromatography (GC). Separation of individual phospholipid classes was performed in lipid extracts from mitochondrial isolates (0.5 mg protein) by normal phase liquid chromatography (Agilent Zorbax Rx-Sil column, 4.6 X 250mm, 5-micron) using a Hexane:Isopropanol:Potassium Acetate mobile phase gradient optimized for separation of cardiolipin, phosphatidylcholine (PC), and phosphatidylethanolamine (PE) by UV detection (206 nm). Fractions were collected based on elution time of known standards, evaporated under a nitrogen stream, and resuspended in hexane, followed by the addition of 14% BF_3 -methanol and heating at 100 $^\circ\text{C}$ for 30 minutes to obtain methyl esters for GC analysis of fatty acid composition. GC analysis was performed using an Agilent Technologies DB-225 30m x 0.250mm x 0.25 μ m column (model 122-2232, J&W Scientific) on an Agilent 6890 Series Gas Chromatographer. The initial temperature of the oven was 120 $^\circ\text{C}$ with an initial ramp temperature of 10 $^\circ\text{C}/\text{min}$ for 8 minutes, then 2.5 $^\circ\text{C}/\text{min}$ for 4 minutes and held at 210 $^\circ\text{C}$ for the remaining 6 minutes for a total run time of 20 min. The inlet split ratio was 15:1 with the column at constant flow and an initial flow, pressure, and velocity at 1.8ml/min, 23.59 psi, and

42 cm/sec, respectively. Fatty acid data are presented as % total fatty acids and D6D product/precursor ratios. Given evidence for a link between membrane peroxidizability index (PI) and lipid peroxidation mammalian lifespan [13, 18], the membrane PI was calculated as: (% monoenoic X 0.025)+ (% dienoic X 1)+(% trienoic X 2)+(% tetraenoic X 4)+(% pentaenoic X 6)+(% hexaenoic X 8).

Mitochondrial respiration

State 3 (ADP-limited; 50 μ M) and state 4 (leak) respiration rates were determined in freshly isolated mitochondria (75 μ g protein) by high resolution respirometry (Oroboros Oxygraph; Innsbruck, Austria) with the saturating concentrations of pyruvate (5mM) + malate (5mM). Respiration studies were conducted at an initial oxygen concentration of 150 μ M at 37C in MiR06 respiration buffer containing (in mM) EGTA (0.5), MgCl₂·6 H₂O (3), K-lactobionate (60), taurine (20), KH₂PO₄ (10), HEPES (20), sucrose (110), 1g/L BSA, 280U/ml catalase, pH 7.4 (with KOH). ADP/O ratio was calculated by dividing the quantity of ADP by oxygen consumed during state 3 respiration as an index of oxidative phosphorylation efficiency. Relative protein expressions of mitochondrial respiratory complexes I-V were determined by standard immunoblotting methods using the OXPHOS antibody complex recognizing subunits from each of the five respiratory complexes (Abcam).

Mitochondrial H₂O₂ release

Mitochondrial ROS release was measured as H₂O₂ in freshly isolated mitochondria (30 μ g protein) using the fluorometric Amplex UltraRed probe (Molecular Probes; 59.1 μ M) in the presence of horseradish peroxidase (HRP; 0.12U/ml) as previously described [19]. Fluorescence

was measured in a microplate reader (SpectraMax M5; Molecular Devices; Sunnyvale, CA, USA) with 560 nm excitation and 590 nm emission wavelengths. Mitochondria were incubated at room temperature in 50mM KH_2PO_4 , pH 7.4. H_2O_2 production was monitored under state 4 conditions in the presence of oligomycin A (5 $\mu\text{g}/\text{mL}$) using succinate (5mM) + rotenone (2.4 μM) (SROA; complex II-linked) and malate (5 mM) + pyruvate (5mM) (MPOA; complex I-linked), over 30 min and presented as total H_2O_2 produced minus background fluorescence using a H_2O_2 standard curve [19].

Mitochondrial lipid peroxidation

To assess the extent of chronic oxidative stress to mitochondria, 30 μg of mitochondrial protein were immunoblotted for 4-hydroxynonenal (HNE)-protein adducts (Calbiochem; catalog #393207; 1:2000 dilution) followed by chemiluminescent detection using a UVP ChemiDoc imager (UVP; Upland, CA, USA).

Echocardiography and Histology

Transthoracic echocardiography was performed under light (1.5%) isoflurane anesthesia immediately prior to and following the 4-week experimental period using a 12 MHz pediatric transducer connected to a Hewlett Packard Sonos 5500 Ultrasound. Short axis 2D images of left ventricular (LV) end-diastolic and end-systolic areas (EDA and ESA, respectively) were obtained for assessment of LV chamber morphology and fractional shortening ((EDA-ESA)/EDA)*100). Data were averaged from five consecutive high-resolution cycles by the same experienced technician. Histology was conducted in 10 μm sections of small (2-3 mm^3) paraffin

embedded LV samples (n = 2-3/group) with Masson's trichrome stain for qualitative assessment of myocardial morphology and fibrosis.

Statistical analyses

All data are presented as group means \pm standard error. Data were analyzed by 2(age) X 2(drug) ANOVA to determine main and interaction effects with Tukey tests *post hoc* for determination of significant group differences. Within-group differences in echocardiography data from pre- to post-treatment were compared by paired t-tests. Statistical significance was established at $P < 0.05$ for all analyses.

Results

Phospholipid fatty acid composition

In the absence of dietary supplementation, desaturation and elongation of linoleic acid and α -linolenic acid provide the majority of long-chain PUFAs present in mammalian tissues. D6D catalyzes the rate-limiting step in this pathway (Fig 2.1); therefore, changes in specific tissue phospholipid PUFA product/precursor ratios (e.g., AA/LA, 20:3n6/LA and DHA/22:5n3) reflect chronic changes in D6D activity *in vivo* [20].

Pilot studies in heart tissues obtained from the NIA tissue bank confirmed a significant 24% loss of 18:2n6 in cardiolipin and total cardiac phospholipids in aged vs. young mice, which corresponded to an increase n-3 and n-6 PUFA product/precursor ratios routinely used as markers of D6D activity (Table 2.1). In our experimental studies, old mice exhibited a similarly significant 21% lower proportion of 18:2n6 and elevated D6D product/precursor ratios in cardiac phospholipids from old vs. young mice (Table 2.3). Treatment with the D6D inhibitor reversed

these effects, increasing 18:2n6 to above young control levels in both young and aged animals, and markedly decreasing dihomo-gamma linolenic acid (20:3n6; DLGA), DHA and D6D product/precursor ratios. Additionally, a similar age-associated loss of 18:2n6 was observed in serum that was reversed by D6D inhibition (Table 2.3).

Age-related changes in cardiolipin composition generally reflected those observed in total myocardial phospholipids, including a significant loss of 18:2n6 paralleled by reciprocal increases in AA, DHA and multiple D6D activity ratios, all of which were reversed by D6D inhibition (Fig 2.2). Effects of aging and D6D inhibition were nearly identical in SSM and IFM (Table 2.2a,b). The redistribution of LA, palmitic and stearic acid for highly unsaturated DHA, AA and DGLA resulted in a significantly higher cardiolipin peroxidation index (PI) in mitochondria from aged hearts, which was reduced to below young control levels by treatment with the D6D inhibitor (Fig 2.2E).

Animal characteristics and cardiac structure/function

Body weights were similar in young (31.8 ± 0.4 g) and old mice (31.4 ± 1.0 g) and were unaffected by treatment with the D6D inhibitor (30.8 ± 0.5 and 31.0 ± 0.9 in young and old, respectively). Heart weight was significantly greater in untreated old (179 ± 8 mg) compared to young mice (142 ± 3 mg), but was significantly lower in old mice treated with the D6D inhibitor (146 ± 3 mg; $P < 0.05$ vs. old). Thus, D6D inhibition ameliorated a 27% higher heart/body weight observed in old vs. young untreated mice (Figure 2.3B). A similar attenuation of age-related cardiac hypertrophy was seen by echocardiography (Figure 2.3A), which revealed a 12% reduction in left ventricular (LV) end-diastolic area in old mice treated with the D6D inhibitor ($P < 0.01$). Moreover, D6D inhibition prevented a 20% decline in LV fractional shortening resulting

in part from a 32% increase in end-systolic area in untreated old mice during the 4-week study, indicating a preservation of LV contractile function. Qualitative histological assessment of LV morphology revealed generally lower myocyte cross-sectional areas and fewer instances of perivascular and interstitial fibrosis in treated vs. untreated old mice (Figure 2.3C). No significant effects of D6D inhibition were seen on cardiac morphology or function in young mice.

Mitochondrial respiration

Significant main effects of aging on mitochondrial state 3 (phosphorylating) respiratory capacity, respiratory control and oxidative phosphorylation efficiency (ADP/O) were seen in IFM, but not SSM (Figure 2.4). D6D inhibition had no effect on respiratory parameters except for a significant increase in ADP/O in old SSM. No significant effects of aging or D6D inhibition were seen on the protein contents of respiratory complex subunits in IFM.

Mitochondria H₂O₂ release and lipid peroxidation

No effects of aging or D6D inhibition were seen on mitochondrial H₂O₂ release from IFM or SSM when pyruvate + malate were provided as substrates (Figure 2.5A). Supplying electrons directly to respiratory complex II with succinate + rotenone substantially increases mitochondrial H₂O₂ release (from complex III) and revealed a significant main effect of aging in both mitochondrial subpopulations (Fig 2.5B). However, this effect was not altered by D6D inhibition. Despite significant changes in mitochondrial phospholipid peroxidation index, no effects of aging or D6D inhibition were seen on mitochondrial 4-HNE-protein adducts.

Discussion

The primary aim of this investigation was to determine if inhibition of essential PUFA metabolism by D6D would ameliorate age-related compositional changes in cardiac cardiolipin, thereby modulating mitochondrial function in the aged heart. Cardiolipin is a glycerolphospholipid with a unique dimeric structure consisting of four fatty acyl chains. It is almost found exclusively in the inner mitochondrial membrane where it provides essential structural and functional support to proteins involved in oxidative phosphorylation [15]. The majority of cardiolipin molecular species in the healthy mammalian heart contain four LA-acyl chains. This LA enrichment is attenuated with aging [8, 14] and age-related diseases such as heart failure [16], and it is this loss of LA enrichment that has been suggested as a potential contributor to mitochondrial dysfunction associated with these conditions. It is well established that the compositional uniformity of cardiolipin results from a series of deacylation and reacylation reactions following *de novo* biosynthesis in mitochondria [15, 21], but the mechanism of decreased LA enrichment seen in aging and age-related diseases remains unclear.

Based on the evidence that the decrease in LA is concomitantly increased with AA and DHA, the long-chain products of the D6D pathway, we hypothesized that the bioavailability of LA is reduced in aging due to the action of D6D pathway. In support of our hypothesis, D6D inhibition reversed the signature PUFA redistribution pattern in CL in aged mice, which restored LA content to levels greater than untreated young and lowered long-chain PUFAs to near or below that of untreated young mice. Similar changes were seen in total myocardial and serum phospholipids, suggesting that changes in CL composition are influenced by a global redistribution of PUFAs in the heart.

The extent to which aging, in the absence of overt pathology, elicits cardiac mitochondrial dysfunction is somewhat controversial, and is at least partially dependent on the models and methods employed [4, 5, 22-24]. We sought to extend information in the area by investigating effects on the two spatially and functionally distinct subpopulations of mitochondria present in cardiomyocytes. As previously reported in rats [5], significant respiratory dysfunction was only seen in IFM of aged mice in our study, manifesting as a main effect of aging to reduce the capacity (state 3), control (RCR) and efficiency (ADP/O) of oxidative phosphorylation. However, restoration of LA-enriched cardiolipin with D6D inhibition had no effect on these parameters in aged or young IFM. Moreover, despite similar age-related compositional changes of cardiolipin, PC and PE in both IFM and SSM, no changes in respiratory parameters were seen in SSM. Interestingly, D6D inhibition significantly improved phosphorylation efficiency in aged SSM, but not in other groups. Taken together, these studies suggest that while age-related changes in mitochondrial phospholipid PUFA composition is a consistent biological phenomenon, it does not appear to be a major independent regulator of mitochondrial respiratory function in the heart. Furthermore, no changes were seen in protein levels of mitochondrial respiratory complex subunits, suggesting that mechanisms other than phospholipid remodeling and respiratory protein deficiency must contribute to impaired respiratory function in aged heart mitochondria.

Mitochondria may also contribute to cardiac aging by increasing release of ROS from the respiratory chain, leading to an accumulation of oxidative damage to cellular components [4, 23]. Exchange of LA for long-chain unsaturated PUFAs in cardiolipin has been associated with increased mitochondrial ROS release in other models [25, 26]; therefore the similar remodeling pattern observed in aged mitochondria may also enhance ROS release and oxidative stress.

During non-phosphorylating (oligomycin A-inhibited) maximal succinate-supported respiration, significant main effects of aging on H₂O₂ release from both SSM and IFM were observed in the present study, which demonstrated a greater capacity to release ROS from intact mitochondria. However, D6D inhibition had no effect on ROS release capacity in young or old mitochondria, arguing against a primary influence of phospholipid remodeling on this process.

Despite evidence for a greater capacity for mitochondrial ROS release with aging, there was no significant increase in mitochondrial oxidative stress assessed by levels of HNE-protein adducts in mitochondria. This was surprising, as the higher unsaturation (or “peroxidizability”) index of mitochondrial phospholipids alone would be expected to promote accumulation of lipid peroxidation species [10, 11, 18]. However, at least two other studies have demonstrated that in the absence of pathology, greater incorporation of highly unsaturated fatty acids into membrane phospholipids does not necessarily elicit the increase in lipid peroxidation as predicted by their peroxidizability index [27, 28]. Importantly, while the capacity for aged mitochondrial to release ROS was elevated in this study, this does not necessarily indicate that ROS production or release was elevated *in vivo*. While evidence supporting greater cardiac mitochondrial oxidative damage in aging is controversial [29], enhanced susceptibility to injury following acute oxidant stress such as ischemia is more consistent [30]. Therefore, it is plausible that age-related unsaturation of membrane phospholipids predisposes the heart to oxidative injury from ROS, but is not sufficient to promote oxidative stress in the absence of pathogenic stimuli.

While reversal of phospholipid remodeling by D6D inhibition was not associated with improved mitochondrial function, the marked attenuation of cardiac hypertrophy and contractile function indicates a potentially protective effect of D6D inhibition on the aged heart. A proportional loss of LA is the most marked age-related change in myocardial and serum

phospholipid composition. The reversibility of this effect by D6D inhibition implicates the conversion of LA into downstream long-chain PUFAs, the most prominent being AA. However, increases in phospholipid AA were not seen to the same magnitude as LA losses in the present study. It may be speculated that the blunted increase in phospholipid AA reflects greater amounts of “free” AA and/or its metabolism by enzymatic and non-enzymatic oxidation pathways capable of generating a host of bioactive eicosanoid species [31, 32]. Enhanced metabolism of AA though these pathways in cardiomyocytes promotes maladaptive cardiac hypertrophy and contractile dysfunction in transgenic mice [33, 34] and hypertrophy in cardiomyocytes [35, 36]. Therefore, increased flux of LA through the D6D pathway may drive pathogenic eicosanoid production and contribute to myocardial remodeling in aging.

In summary, we have shown that inhibiting the D6D pathway can restore the loss of LA enrichment of cardiolipin seen in the aging heart, implicating PUFA metabolism as an important determinant of cardiolipin composition in the heart. Additionally, despite close correlation, there appears to be no independent effect of altered cardiolipin composition on cardiac mitochondrial respiratory function and oxidative stress in aging, but it reflects global changes in PUFA metabolism that appear to have important effects on myocardial remodeling and function. Future studies are needed to explore the mechanisms of this effect and perhaps other pathophysiological manifestations of phospholipid remodeling in aging and related pathologies.

Table 2.1. Acyl composition of total myocardial phospholipids and cardiolipin in young and old C57BL/6 hearts (obtained from NIA tissue bank)

	Total Phospholipids		Cardiolipin Fraction	
	4mo	24mo	4mo	24mo
16:0, Palmitic	13.36 ± 0.06	13.67 ± 0.00	3.79 ± 0.21	6.00 ± 0.15*
18:0, Stearic	19.33 ± 0.20	18.95 ± 0.16	8.28 ± 0.94	12.25 ± 1.67
18:1n9, Oleic	5.52 ± 0.55	4.83 ± 0.08	8.37 ± 1.06	11.03 ± 1.91
18:1n7, Vaccenic	2.07 ± 0.14	2.61 ± 0.01	3.60 ± 0.01	5.86 ± 0.62*
18:2n6, Linoleic	18.23 ± 0.35	13.68 ± 0.10*	63.27 ± 4.84	43.26 ± 1.77*
18:3n3, Linolenic	0.15 ± 0.01	.018 ± 0.04	1.21 ± 0.12	1.21 ± 0.09
20:3n6, DHGLA	0.86 ± 0.05	.098 ± 0.02*	3.44 ± 0.31	3.77 ± 0.19
20:4n6, AA	8.60 ± 0.31	7.40 ± 0.14*	1.05 ± 0.11	1.24 ± 0.24
22:5n3, DPA	1.67 ± 0.02	1.49 ± 0.11*	ND	ND
22:6n3, DHA	28.75 ± 0.28	35.10 ± 0.23*	4.16 ± 0.50	12.60 ± 0.18*
20:4n6/18:2n6	0.47 ± 0.01	0.54 ± 0.01*	0.02 ± 0.00	0.03 ± 0.00*
20:3n6/18:2n6X100	4.73 ± 0.17	7.18 ± 0.08*	5.47 ± 0.46	8.73 ± 0.39*
22:6n3/22:5n3	17.18 ± 0.35	23.78 ± 1.65*	N/A	N/A
22:6n3/18:3n3	193 ± 5.29	209 ± 42	3.49 ± 0.58	10.42 ± 0.24*
PI	295 ± 3.81	336 ± 2.15*	110 ± 2	160 ± 2*
n6/n3	0.91 ± 0.02	0.60 ± 0.01*	12.85 ± 1.48	3.49 ± 0.01*

All data are means ± SEM of % total fatty acids or calculated D6D product/precursor indices (n = 4-6/group). PI = peroxidizability index calculated as in Methods; n6/n3 ratio is the sum %total of all n6/n3 PUFAs detected in the sample. Main effects of aging, D6D inhibition (SC) and their interaction by ANOVA are indicated by their respective P values. *P < 0.05 vs. 4 mo.

Table 2.2a. Acyl composition of PC and PE in subsarcolemmal mitochondria

	<u>Young</u>	<u>Young+SC</u>	<u>Old</u>	<u>Old+SC</u>	<u>Age</u>	<u>SC</u>	<u>Int</u>
<i>Phosphatidylcholine</i>	(%)	(%)	(%)	(%)	(P)	(P)	(P)
16:0, Palmitic	16.33 ± 0.40	15.71 ± 1.20	15.52 ± 1.94	18.08 ± 1.21	0.551	0.009*	0.002*
18:0, Stearic	21.20 ± 0.78	22.45 ± 0.18	23.86 ± 1.41	22.96 ± 0.52	0.314	0.404	0.422
18:1n9, Oleic	7.64 ± 0.50	7.93 ± 0.63	6.88 ± 0.42	9.99 ± 0.49	0.112	0.001*	0.001*
18:1n7, Vaccenic	1.82 ± 0.12	2.83 ± 0.28	2.51 ± 0.16	2.87 ± 0.17	0.022*	0.003*	0.019*
18:2n6, Linoleic	8.88 ± 0.52	18.92 ± 1.26	9.06 ± 0.68	15.45 ± 1.75	0.146	0.000*	0.288
18:3n3, Linolenic	0.18 ± 0.02	0.23 ± 0.03	0.28 ± 0.04	0.28 ± 0.06	0.117	0.748	0.130
20:3n6, DHGLA	0.62 ± 0.05	0.86 ± 0.04	0.60 ± 0.01	0.62 ± 0.09	0.113	0.050*	0.147
20:4n6, AA	9.71 ± 0.32	8.50 ± 0.51	12.19 ± 1.06	10.64 ± 0.35	0.000*	0.000*	0.046*
22:5n3, DPA	2.52 ± 0.34	2.18 ± 0.09	1.39 ± 0.16	0.98 ± 0.10	0.001*	0.084	0.615
22:6n3, DHA	29.15 ± 1.00	20.40 ± 2.13	24.69 ± 2.36	17.06 ± 2.59	0.008*	0.000*	0.190
20:4n6/18:2n6	1.11 ± 0.08	0.45 ± 0.06	1.38 ± 0.19	0.73 ± 0.11	0.002*	0.000*	0.086
20:3n6/18:2n6X100	7.02 ± 0.54	1.20 ± 0.28	6.71 ± 0.55	4.12 ± 0.59	0.608	0.000*	0.428
22:6n3/22:5n3	12.23 ± 1.57	9.37 ± 0.75	17.99 ± 1.42	17.33 ± 1.23	0.001*	0.134	0.769
22:6n3/18:3n3	168 ± 20	90 ± 4	95 ± 18	63 ± 6	0.028*	0.011*	0.233
PI	298 ± 8	232 ± 15	287 ± 11	184 ± 10	0.017*	0.000*	0.101
n6/n3	0.61 ± 0.03	1.24 ± 0.10	0.78 ± 0.01	1.83 ± 0.20	0.007*	0.000*	0.093
<i>Phosphatidylethanolamine</i>							
16:0, Palmitic	8.06 ± 0.86	7.26 ± 0.27	8.27 ± 0.43	13.56 ± 3.21	0.300	0.511	0.292
18:0, Stearic	25.46 ± 0.96	29.29 ± 0.36	26.16 ± 0.52	29.90 ± 1.12	0.568	0.002*	0.378
18:1n9, Oleic	7.79 ± 0.62	6.39 ± 0.29	7.95 ± 0.42	8.36 ± 0.43	0.088	0.717	0.046*
18:1n7, Vaccenic	0.81 ± 0.06	0.93 ± 0.05	1.37 ± 0.04	1.07 ± 0.05	0.000*	0.041*	0.004*
18:2n6, Linoleic	3.81 ± 0.13	6.87 ± 0.53	3.33 ± 0.03	5.73 ± 0.50	0.025*	0.000*	0.124
18:3n3, Linolenic	0.35 ± 0.08	0.19 ± 0.01	0.33 ± 0.05	0.26 ± 0.10	0.346	0.260	0.293
20:3n6, DHGLA	0.26 ± 0.02	0.38 ± 0.01	0.30 ± 0.01	0.32 ± 0.05	0.007*	0.074	0.001*
20:4n6, AA	7.25 ± 0.37	7.99 ± 0.21	9.05 ± 0.21	8.75 ± 0.60	0.046*	0.743	0.179
22:5n3, DPA	1.79 ± 0.25	1.84 ± 0.05	1.05 ± 0.09	0.78 ± 0.07	0.001*	0.326	0.676
22:6n3, DHA	41.70 ± 0.88	38.87 ± 1.07	37.80 ± 0.94	29.61 ± 3.21	0.043*	0.074	0.569
20:4n6/18:2n6	1.92 ± 0.15	1.16 ± 0.07	2.72 ± 0.07	1.53 ± 0.09	0.001*	0.000*	0.131
20:3n6/18:2n6X100	5.32 ± 1.80	2.83 ± 0.15	8.90 ± 0.44	5.65 ± 0.70	0.487	0.001*	0.049*
22:6n3/22:5n3	24.48 ± 2.81	21.18 ± 1.17	36.57 ± 2.35	37.89 ± 2.56	0.000*	0.508	0.285
22:6n3/18:3n3	138 ± 27	200 ± 11	129 ± 26	149 ± 41	0.043*	0.152	0.182
PI	378 ± 8	362 ± 12	353 ± 9	306 ± 34	0.059	0.122	0.490
n6/n3	0.26 ± 0.00	0.37 ± 0.01	0.32 ± 0.01	0.41 ± 0.01	0.001*	0.000*	0.103

All data are means ± SEM of % total fatty acids or calculated D6D product/precursor indices (n = 4-6/group). PI = peroxidizability index calculated as in Methods; n6/n3 ratio is the sum %total of all n6/n3 PUFAs detected in the sample. Main effects of aging, D6D inhibition (SC) and their interaction by ANOVA are indicated by their respective P values. *P < 0.05.

Table 2.2b. Acyl composition of PC and PE in intermyofibrillar mitochondria

	Young	Young+SC	Old	Old+SC	Age	SC	Int
<i>Phosphatidylcholine</i>	(%)	(%)	(%)	(%)	(P)	(P)	(P)
16:0, Palmitic	15.99 ± 0.60	16.94 ± 1.29	17.53 ± 3.20	17.01 ± 0.17	0.418	0.333	0.164
18:0, Stearic	20.24 ± 0.46	21.27 ± 0.17	21.29 ± 0.29	20.23 ± 0.30	0.909	0.927	0.010*
18:1n9, Oleic	4.91 ± 0.25	5.02 ± 0.40	5.88 ± 0.44	11.5 ± 0.31	0.000*	0.000*	0.000*
18:1n7, Vaccenic	1.84 ± 0.13	1.74 ± 0.17	2.52 ± 0.15	2.88 ± 0.12	0.023*	0.127	0.844
18:2n6, Linoleic	9.78 ± 0.87	14.64 ± 0.97	8.32 ± 0.88	15.18 ± 1.04	0.184	0.000*	0.576
18:3n3, Linolenic	0.16 ± 0.02	0.19 ± 0.03	0.10 ± 0.08	0.12 ± 0.01	0.002*	0.134	0.239
20:3n6, DHGLA	0.62 ± 0.07	0.54 ± 0.02	0.54 ± 0.03	0.57 ± 0.03	0.020*	0.629	0.970
20:4n6, AA	10.43 ± 0.28	8.34 ± 0.50	12.76 ± 0.60	11.66 ± 0.64	0.000*	0.008*	0.412
22:5n3, DPA	2.55 ± 0.38	2.09 ± 0.09	1.60 ± 0.12	1.07 ± 0.05	0.000*	0.038*	0.870
22:6n3, DHA	31.44 ± 1.32	26.06 ± 2.72	26.71 ± 2.88	18.63 ± 1.41	0.038*	0.000*	0.821
20:4n6/18:2n6	1.09 ± 0.11	0.60 ± 0.08	1.90 ± 0.36	0.78 ± 0.06	0.001*	0.000*	0.151
20:3n6/18:2n6X100	6.49 ± 0.81	5.27 ± 1.21	8.07 ± 1.56	3.78 ± 0.15	0.285	0.000*	0.741
22:6n3/22:5n3	13.30 ± 2.24	13.42 ± 1.07	17.79 ± 1.23	17.39 ± 1.08	0.003*	0.692	0.496
22:6n3/18:3n3	204 ± 29	137 ± 6.56	237 ± 68	162 ± 9	0.019*	0.008*	0.682
PI	320 ± 10	248 ± 21	284 ± 3.76	219 ± 9.14	0.050*	0.000*	0.932
n6/n3	0.61 ± 0.04	1.04 ± 0.13	0.76 ± 0.01	1.42 ± 0.16	0.035*	0.000*	0.208
<i>Phosphatidylethanolamine</i>							
16:0, Palmitic	7.12 ± 0.51	6.78 ± 0.25	9.85 ± 2.35	9.14 ± 2.51	0.218	0.992	0.639
18:0, Stearic	25.68 ± 0.26	26.52 ± 0.32	25.69 ± 0.60	26.92 ± 0.45	0.104	0.003*	0.962
18:1n9, Oleic	5.72 ± 0.14	5.76 ± 0.26	6.37 ± 0.16	10.36 ± 0.48	0.000*	0.000*	0.000*
18:1n7, Vaccenic	0.86 ± 0.07	0.77 ± 0.04	1.26 ± 0.04	1.12 ± 0.10	0.013*	0.588	0.273
18:2n6, Linoleic	3.89 ± 0.16	5.45 ± 0.42	3.13 ± 0.23	6.31 ± 0.35	0.083	0.000*	0.080
18:3n3, Linolenic	0.08 ± 0.01	0.05 ± 0.00	0.09 ± 0.10	0.15 ± 0.06	0.603	0.914	0.631
20:3n6, DHGLA	0.24 ± 0.02	0.19 ± 0.01	0.25 ± 0.00	0.22 ± 0.02	0.082	0.561	0.462
20:4n6, AA	7.52 ± 0.19	6.86 ± 0.18	8.67 ± 0.08	9.35 ± 0.50	0.004*	0.348	0.299
22:5n3, DPA	1.80 ± 0.29	1.67 ± 0.05	1.21 ± 0.05	0.87 ± 0.04	0.000*	0.257	0.371
22:6n3, DHA	44.27 ± 0.53	43.01 ± 1.18	39.74 ± 2.13	33.80 ± 2.25	0.003*	0.015*	0.091
20:4n6/18:2n6	1.94 ± 0.10	1.28 ± 0.07	3.03 ± 0.27	1.50 ± 0.12	0.001*	0.000*	0.013*
20:3n6/18:2n6X100	6.13 ± 0.56	3.07 ± 0.16	8.73 ± 0.84	3.47 ± 0.24	0.404	0.000*	0.024*
22:6n3/22:5n3	26.71 ± 4.62	28.09 ± 1.56	34.88 ± 2.06	38.88 ± 2.20	0.001*	0.000*	0.325
22:6n3/18:3n3	577 ± 41	578 ± 32	367 ± 107	337 ± 85	0.687	0.693	0.384
PI	400 ± 4	390 ± 6	375 ± 17	320 ± 18	0.003*	0.025*	0.108
n6/n3	0.25 ± 0.00	0.33 ± 0.03	0.28 ± 0.01	0.46 ± 0.04	0.005*	0.000*	0.018*

All data are means ± SEM of % total fatty acids or calculated D6D product/precursor indices (n = 4-6/group). PI = peroxidizability index calculated as in Methods; n6/n3 ratio is the sum %total of all n6/n3 PUFAs detected in the sample. Main effects of aging, D6D inhibition (SC) and their interaction by ANOVA are indicated by their respective P values. *P < 0.05.

Table 2.3. Acyl composition of myocardial and serum phospholipids

	Young	Young+SC	Old	Old+SC	Age	SC	Int
Heart	(%)	(%)	(%)	(%)	(P)	(P)	(P)
16:0, Palmitic	13.07 ± 0.25	14.78 ± 0.26	13.01 ± 0.27	12.20 ± 0.59	0.020*	0.362	0.024*
18:0, Stearic	19.26 ± 0.15	21.67 ± 0.31	20.74 ± 0.10	20.69 ± 0.27	0.325	0.001*	0.001*
18:1n9, Oleic	5.33 ± 0.43	5.67 ± 0.08	6.10 ± 1.00	6.60 ± 1.19	0.441	0.701	0.943
18:1n7, Vaccenic	2.14 ± 0.11	2.19 ± 0.04	2.53 ± 0.23	2.16 ± 0.21	0.427	0.485	0.343
18:2n6, Linoleic	18.99 ± 0.71	23.50 ± 0.04*	14.92 ± 0.42	20.57 ± 0.67	0.000*	0.000*	0.404
18:3n3, Linolenic	0.15 ± 0.01	0.14 ± 0.00	0.11 ± 0.02	0.22 ± 0.08	0.712	0.455	0.308
20:3n6, DHGLA	0.94 ± 0.07	0.72 ± 0.00	0.80 ± 0.01	0.59 ± 0.02	0.011*	0.001*	0.959
20:4n6, AA	8.89 ± 0.34	6.95 ± 0.04	9.52 ± 0.45	9.49 ± 0.61	0.016*	0.099	0.109
22:5n3, DPA	1.65 ± 0.03	1.67 ± 0.02	1.29 ± 0.16	1.23 ± 0.18	0.040*	0.919	0.798
22:6n3, DHA	28.09 ± 0.61	22.22 ± 0.60	28.14 ± 1.90	24.17 ± 1.06	0.524	0.010*	0.546
20:4n6/18:2n6	0.47 ± 0.01	0.30 ± 0.00	0.64 ± 0.03	0.46 ± 0.03	0.000*	0.000*	0.942
20:3n6/18:2n6X100	0.49 ± 0.02	0.31 ± 0.00	0.54 ± 0.02	0.29 ± 0.02	0.515	0.000*	0.129
22:6n3/22:5n3	17.08 ± 0.27	13.29 ± 0.19	22.43 ± 1.81	20.63 ± 2.26	0.010*	0.183	0.621
22:6n3/18:3n3	184 ± 9	163 ± 8	262 ± 35	181 ± 62	0.348	0.315	0.546
PI	292 ± 5	242 ± 5	288 ± 15	261 ± 8	0.487	0.008*	0.326
n6/n3	0.97 ± 0.05	1.29 ± 0.03	0.87 ± 0.08	1.21 ± 0.09	0.287	0.003*	0.970
Serum							
16:0, Palmitic	25.19 ± 0.79	24.68 ± 0.40	24.08 ± 0.45	22.90 ± 0.47	0.062	0.237	0.627
18:0, Stearic	16.62 ± 0.42	21.63 ± 1.02	18.22 ± 0.57	21.06 ± 0.61	0.515	0.001*	0.184
18:1n9, Oleic	6.80 ± 0.56	5.33 ± 0.18	9.68 ± 0.64	12.26 ± 1.75	0.007*	0.699	0.178
18:1n7, Vaccenic	1.97 ± 0.54	1.08 ± 0.04	2.50 ± 0.12	1.64 ± 0.23	0.177	0.045	0.965
18:2n6, Linoleic	30.21 ± 0.27	30.54 ± 0.46	23.74 ± 0.75	28.71 ± 0.98	0.002*	0.017*	0.030*
18:3n3, Linolenic	0.17 ± 0.01	0.25 ± 0.03	0.21 ± 0.02	0.20 ± 0.05	0.861	0.416	0.328
20:3n6, DHGLA	1.46 ± 0.12	1.30 ± 0.00	1.62 ± 0.10	1.06 ± 0.14	0.803	0.034*	0.191
20:4n6, AA	11.16 ± 0.24	8.44 ± 0.03	12.98 ± 1.24	6.92 ± 0.40	0.856	0.001*	0.073
20:5n3, EPA	0.17 ± 0.03	0.18 ± 0.02	0.17 ± 0.03	0.16 ± 0.02	0.791	0.846	0.694
22:5n3, DPA	0.28 ± 0.02	0.39 ± 0.01	0.23 ± 0.02	0.20 ± 0.01	0.000*	0.085	0.006*
22:6n3, DHA	5.88 ± 0.06	6.18 ± 0.04	6.49 ± 0.11	4.71 ± 0.43	0.221	0.051	0.012*
20:4n6/18:2n6X10	3.69 ± 0.05	2.79 ± 0.03	5.53 ± 0.68	2.41 ± 0.09	0.109	0.001*	0.023*
20:3n6/18:2n6X100	4.81 ± 0.39	4.25 ± 0.07	6.82 ± 0.40	3.71 ± 0.51	0.184	0.006*	0.035*
22:6n3/22:5n3	21.30 ± 1.29	16.04 ± 0.63	28.23 ± 2.29	23.61 ± 2.84	0.022*	0.104	0.950
22:6n3/18:3n3	34.37 ± 1.44	25.55 ± 3.66	31.65 ± 2.28	30.42 ± 9.56	0.887	0.511	0.618
PI	128 ± 2	120 ± 6	134 ± 5	99 ± 3	0.071	0.000*	0.006*
n6/n3	6.59 ± 0.13	5.76 ± 0.30	5.40 ± 0.03	7.09 ± 0.68	0.892	0.419	0.036*

All data are means ± SEM of % total fatty acids or calculated D6D product/precursor indices (n = 4-6/group). PI = peroxidizability index calculated as in Methods; n6/n3 ratio is the sum %total of all n6/n3 PUFAs detected in the sample. Main effects of aging, D6D inhibition (SC) and their interaction by ANOVA are indicated by their respective P values. *P < 0.05.

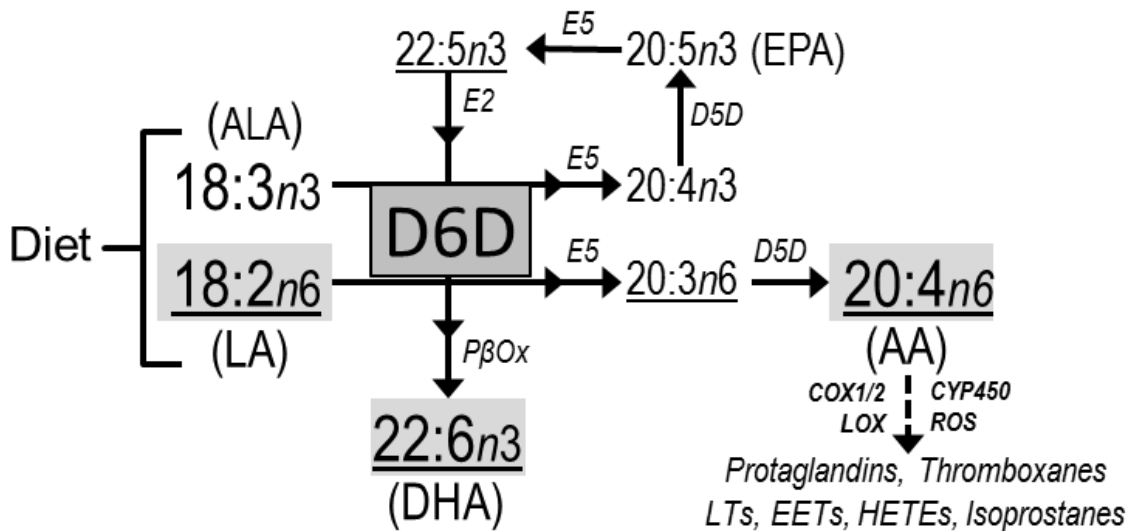


Figure 2.1. Central role of D6D in PUFA metabolism

Delta-6 desaturase (D6D) catalyzes rate-limiting steps in the production of long chain PUFAs from linoleic (18:2n6, LA) and linolenic (18:3n3) acids obtained in the diet. Fatty acid nomenclature: C:XnY where C = number of carbons, X = number of double bonds, and Y = location of first double bond from the omega carbon. Double arrows indicate additional reactions catalyzed by elongase enzymes (E), delta-5 desaturase (D5D) and peroxisomal fatty acid β-oxidation (PβOx). LA, AA and DHA (shaded) are the only PUFAs that readily accumulate in cardiac phospholipids to >2% of total fatty acids in humans and rats. Underscored fatty acids are pathway products or precursors routinely used to estimate D6D activity in tissues. AA serves as the substrate for lipoxygenase (LO), cyclooxygenase (COX), and CYP450 epoxygenase enzymes, or may be non-enzymatically oxidized by reactive oxygen species (ROS), generating an array of bioactive eicosanoid species.

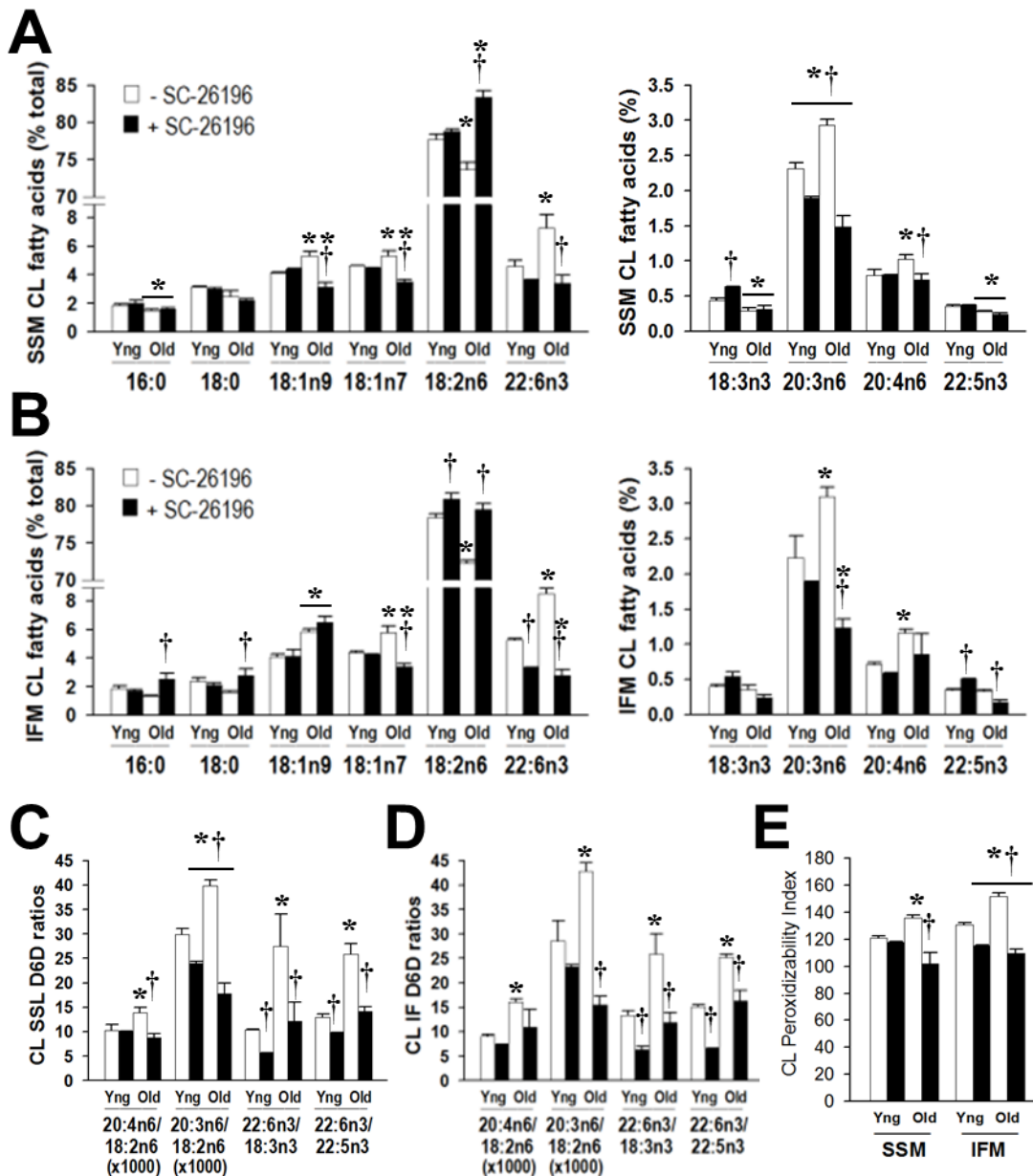


Figure 2.2. D6D inhibition reverses age-related cardiolipin remodeling

Gas chromatographic analysis of cardiolipin fatty acid composition in SSM (A) and IFM (B). Aging elicited significant increases in D6D product/precursor ratio in SSM (C) and IFM (D), as well as the cardiolipin peroxidizability index (E), all of which were reversed by D6D inhibition with SC-26196. *P < 0.05 vs. Pre (within group); †P < 0.05 vs. Old.

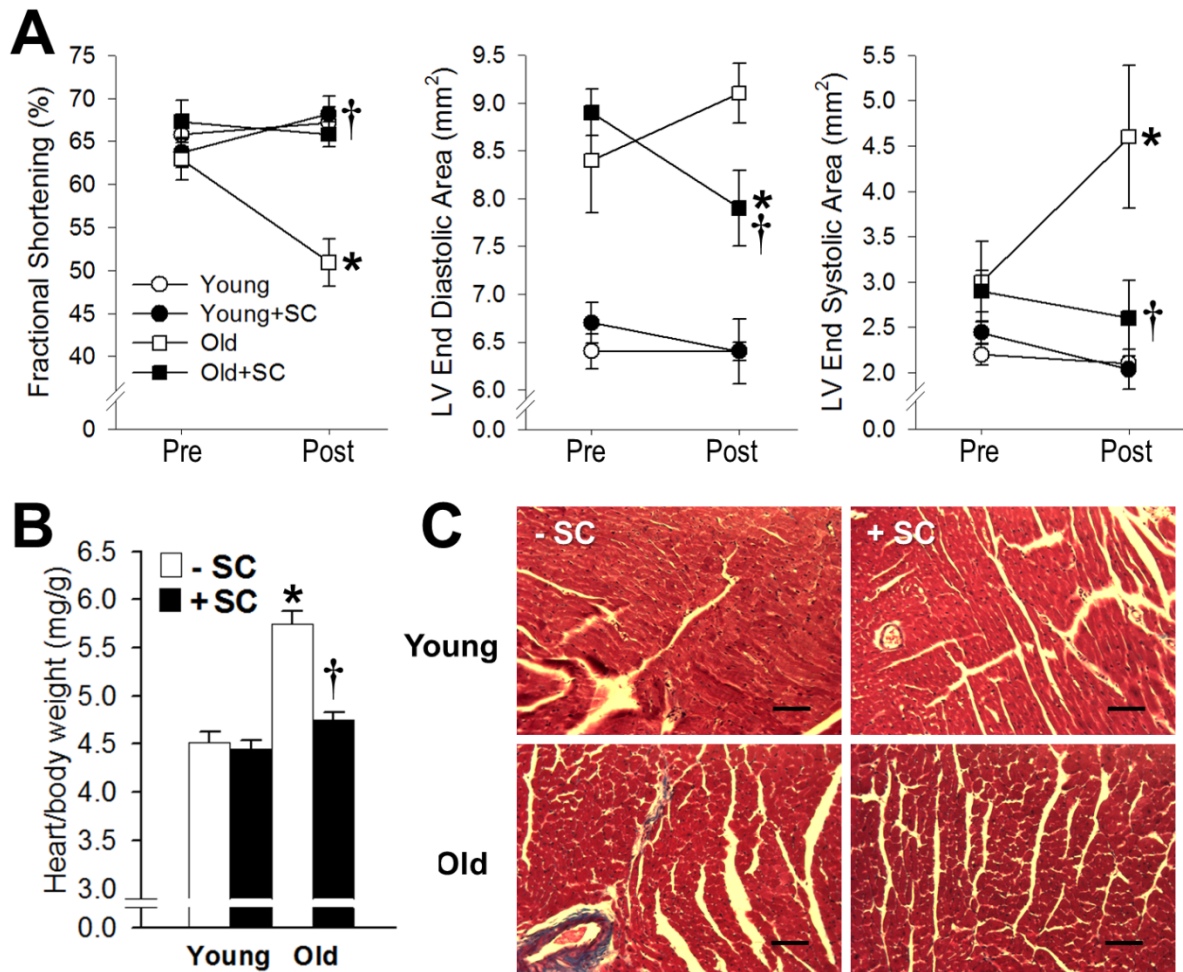


Figure 2.3. D6D inhibition attenuates age-related cardiac hypertrophy and contractile dysfunction

A) Echocardiography revealed left ventricular dilatation (increased LV end diastolic area) and systolic dysfunction (decreased fractional shortening and reduced end systolic area) in old compared to young mice, which was prevented or reversed by D6D inhibition. B) Heart/body weight ratio was elevated in old untreated mice (-SC; n=6), but similar to young in old mice treated with the D6D inhibitor (+SC; n=6). *P < 0.05 vs. Pre (within group); †P < 0.05 vs. Old. C) Representative images of Masson's trichrome stained LV sections from each of the experimental groups (scale bar = 100 μ m).

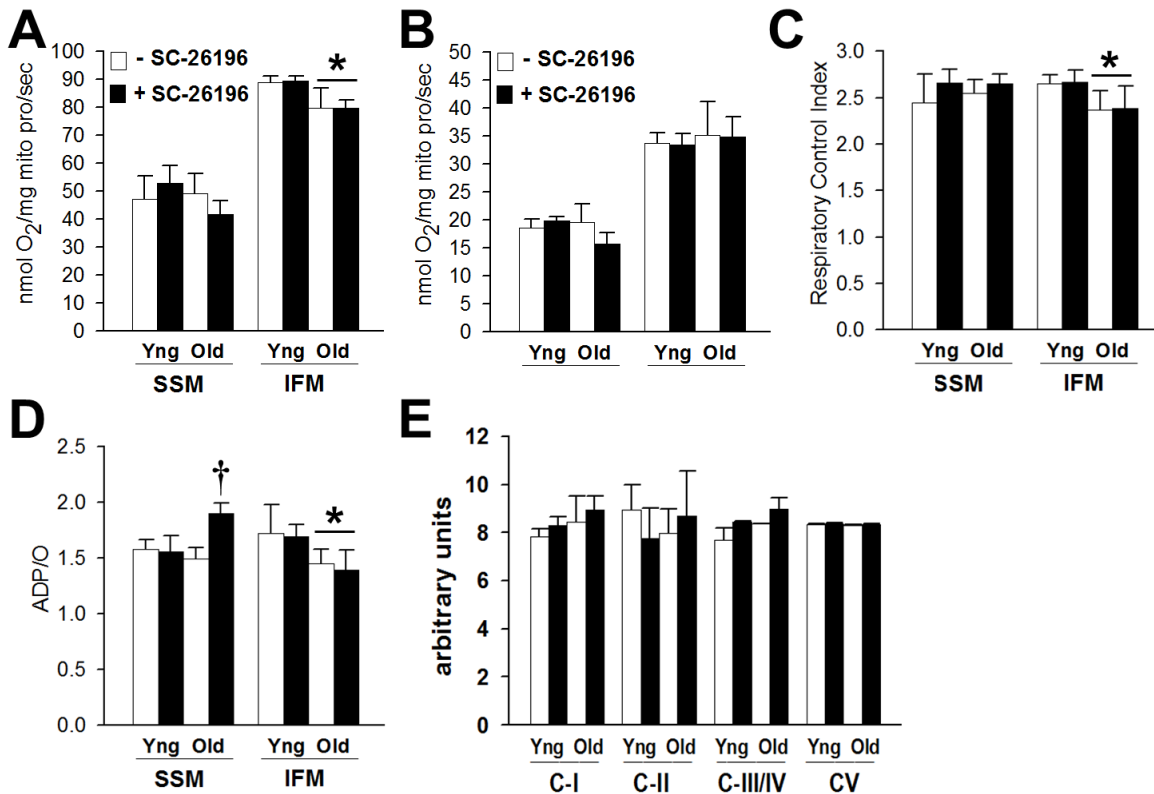


Figure 2.4. Mitochondrial Respiration

Respiratory function of isolated cardiac mitochondria from control (white bars) and D6D inhibition groups (black bars). A) State 3 (ADP-limited) respiration; B) state 4 (uncoupled) respiration; C) Respiratory control ratio (RCR, state3/4) and D) phosphorylation efficiency (ADP phosphorylated per O₂ consumed, ADP/O) (n = 4-6/group). E) Protein expression of subunits from respiratory complexes I-V obtained by immunoblotting 10ug of mitochondrial protein (n = 4/group). *P < 0.05 vs. Pre (within group); †P < 0.05 vs. Old

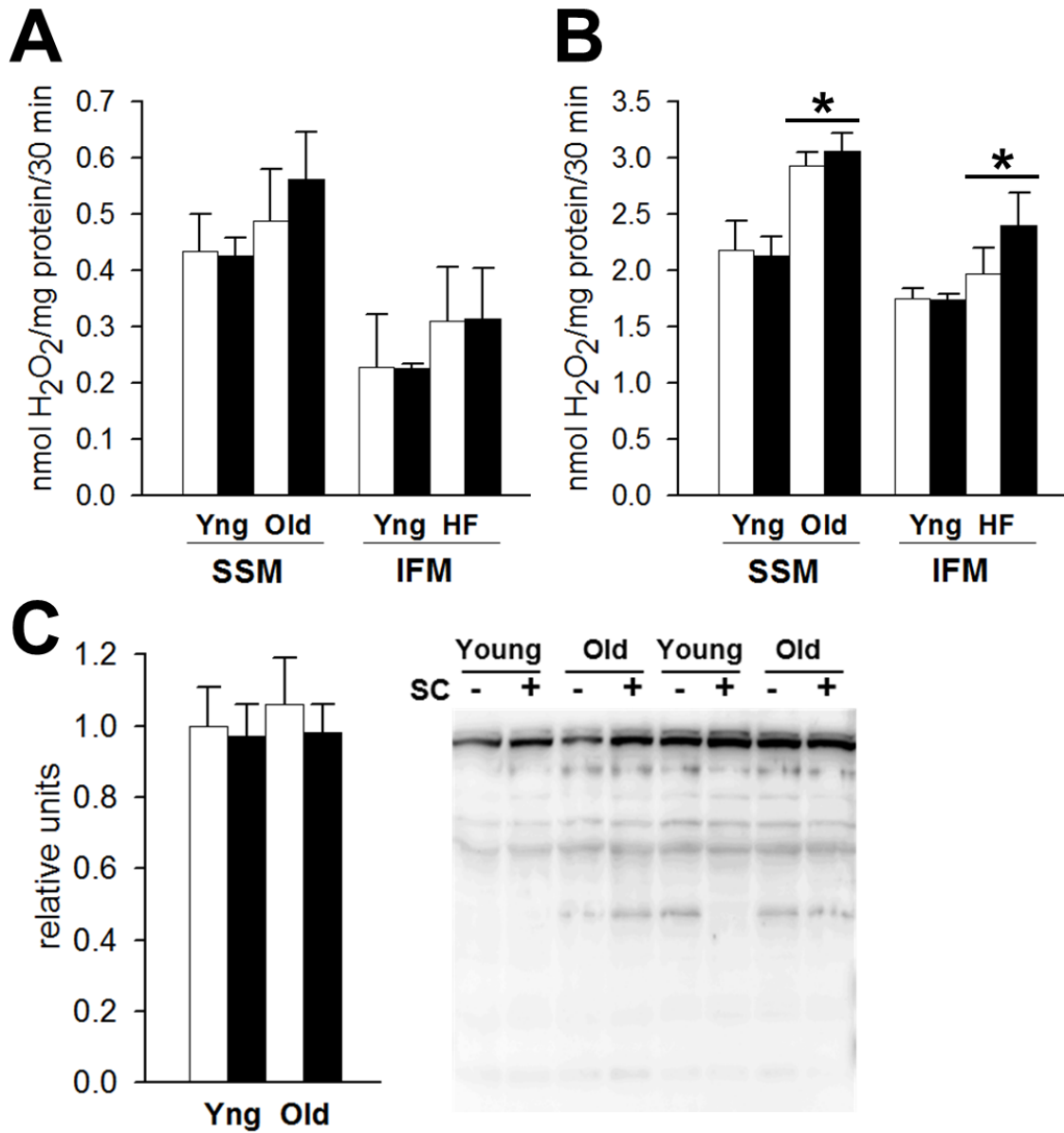


Figure 2.5. Mitochondrial oxidative stress

A) Mitochondrial H₂O₂ release using malate + pyruvate (MPOA; n = 6) or succinate + rotenone (SROA; n = 6) and as substrates in subsarcolemmal (SSM) and intermyofibrillar mitochondria (IFM). B) Maximal rates of mitochondrial H₂O₂ release using succinate + rotenone in the presence of antimycin A (SROA+AA; n = 6). C) Densitometry and representative blotting of mitochondrial 4-HNE-protein adducts from IF mitochondria (n = 8). All data are means ± SEM. *P < 0.05 for main effect of aging.

**Delta-6-desaturase links PUFA metabolism with phospholipid remodeling
and disease progression in heart failure²**

Summary

Alterations in the fatty acid composition of myocardial phospholipids have been reported in various forms of heart failure, but the mechanism and pathophysiological relevance of this phenomenon have remained unclear. Here, we examined the hypothesis that delta-6 desaturase (D6D), the rate limiting enzyme in long-chain polyunsaturated fatty acid (PUFA) biosynthesis, mediates the signature pattern of fatty acid redistribution observed in myocardial phospholipids following chronic pressure overload, and explored plausible links between this process and disease pathogenesis.

Compositional analysis of phospholipids from hearts explanted from patients with dilated cardiomyopathy revealed increases in PUFA product/precursor ratios reflective of D6D hyperactivity, manifesting primarily a loss of linoleic acid with reciprocal increases in arachidonic and docosahexaenoic acids. Chronic mechanical unloading with a left ventricular assist device

² Catherine H. Le^{*}, Christopher M. Mulligan⁺, Melissa A. Routh^{*},
Gerrit J. Bouma[#], Melinda A. Frye[#], Kimberly M. Jeckel[#],
Genevieve C. Sparagna[^], Joshua M. Lynch[^], Russell L. Moore[^],
Sylvia A. McCune[^], Michael Bristow[^], Simona Zarini[◇],
Robert C. Murphy[◇], Adam J. Chicco^{*+##†}

^{*}Program in Cell and Molecular Biology, Departments of ⁺Food Science and Human Nutrition, [#]Biomedical Sciences, and [†]Health and Exercise Science, Colorado State University, Fort Collins, CO; [^]Department of Integrative Physiology, University of Colorado, Boulder, CO; [△]Division of Cardiology and [◇]Department of Pharmacology, University of Colorado at Denver, Denver, CO.

largely reversed this pattern of remodeling. Chronic inhibition of D6D *in vivo* reversed similar patterns of myocardial PUFA redistribution in rat models of pressure overload and hypertensive heart disease, and significantly attenuated cardiac hypertrophy, fibrosis and contractile dysfunction in both models. D6D inhibition also reversed myocardial elevations in pathogenic eicosanoid species, lipid peroxidation, and ERK1/2 activation. Moreover, D6D inhibition normalized cardiolipin composition in mitochondria and reduced circulating levels of inflammatory cytokines. Model-specific effects on cardiac mitochondrial respiratory efficiency, NF κ B activation and caspase activities were also observed. These studies demonstrate a pivotal role of essential fatty acid metabolism through D6D in myocardial phospholipid remodeling induced by hemodynamic stress, and reveal novel links between this phenomenon and the propagation of multiple pathogenic systems involved in maladaptive remodeling and disease progression.

Introduction

Data from chapter II showed loss of linoleic acid in cardiolipin occurred in conjunction with myocardial hypertrophy and impairments in both contractile function and mitochondrial respiratory function in the aged heart. Pharmacological inhibition of delta-6 desaturase reversed cardiolipin remodeling, reduced myocardial hypertrophy and restored contractile function. However, in contrast to our hypothesis, reversal of these changes in cardiolipin composition did not have a significant effect on relatively minor depression of mitochondrial respiratory function in aged hearts. This dissociation between mitochondrial respiratory function and fatty acid composition of cardiolipin led to the possibility that perhaps the cardiac pathology in aging was not severe enough to observe the effects of cardiolipin compositional changes on mitochondrial

respiratory function. Therefore, herein, we examined models of chronic cardiac pathology in a pressure overload and hypertensive heart disease.

Heart failure is a complex, multifactorial syndrome characterized by progressive cardiac remodeling and contractile dysfunction that leads to an impaired matching of blood supply to tissue demands. While the etiology of heart failure is multifaceted and complex, antecedent hypertension is present in the majority of cases [37]. This has led to the widely accepted view that chronic hemodynamic overload of the myocardium results in initially compensatory adaptations that ultimately become maladaptive, leading to pathologic hypertrophy, fibrosis and mechanical failure. Several well-established pathogenic systems have been implicated in the transition from adaptive cardiac hypertrophy to maladaptive remodeling and failure, including chronic inflammation [38], oxidative stress [39], impaired myocardial energetics [40] and apoptosis [41]. However, the molecular triggers and precise contribution of these processes remain areas of intense investigation and debate.

Alterations in the fatty acid composition of myocardial phospholipids have been reported in various forms of cardiac pathology for over 25 years, including human cardiomyopathies [16, 42] and animal models of pressure overload hypertrophy [16, 43], hypertensive heart disease [16, 44], post-infarct remodeling [45], diabetic cardiomyopathy [46], and aging [8]. Interestingly, despite distinct etiologies and genetic backgrounds, the pattern of phospholipid remodeling has consistently manifested as a proportional loss of the essential polyunsaturated fatty acid linoleic acid, often paralleled by reciprocal increases in long chain highly unsaturated fatty acids such as arachidonic acid and/or docosahexaenoic acid. While several hypotheses have been proposed, the mechanism and pathophysiological relevance of this phenomenon have remained areas of speculation.

The present study explored the hypothesis that the redistribution of phospholipid PUFAs in the pressure overloaded and failing heart results from increased activity of delta-6 desaturase (D6D), the rate-limiting enzyme in the production of long-chain PUFAs such as AA and DHA from LA and α -linolenic acid, respectively [47] (Fig 2.1). Furthermore, the aim of the present investigation sought to elucidate the role of cardiac mitochondrial respiratory function in the failing heart and if inhibition of the PUFA redistribution in cardiolipin would restore both mitochondrial respiratory function and cardiac contractile function. Herein, we investigated the effects of chronic pharmacological D6D inhibition in rodent models of pressure overload hypertrophy and hypertensive heart disease and present the first comprehensive analysis of phospholipid composition in the failing human heart with and without mechanical unloading support. These studies reiterate the disassociation between cardiolipin fatty acid composition and mitochondrial respiratory function in the heart. Moreover, these data demonstrate a central role of D6D in myocardial phospholipid remodeling resulting from hemodynamic stress and reveal novel links between this process and disease progression at the molecular, organ, and systemic levels.

Experimental Procedures

Human Heart Tissue

Left ventricular tissue was obtained by an Institutional Review Board-approved protocol maintained by the University of Colorado Denver Cardiac Tissue Bank. Hearts donated for research purposes were obtained under written consent from family members of organ donors or by direct written consent from patients undergoing cardiac transplantation.

Animal Models

Lean male spontaneously hypertensive heart failure ($Mcc^{facp^{-/-}}$; SHHF) rats were obtained from a colony maintained at the University of Colorado. SHHF rats were selected for these studies based on their well-characterized development of progressive hypertensive cardiomyopathy that shares many of the hallmark biochemical and pathophysiological features of DCM in humans[48]. Two cohorts of animals were studied: 1) at 21-22 months of age when rats exhibit pathologic cardiac hypertrophy progressing toward dilated heart failure (HF), and 2) following thoracic aortic banding at 3 months of age to induce hemodynamic stress and pathologic hypertrophy in the absence of age-related pathology (TAC)[16]. Cohorts of HF and TAC (2 weeks post-surgery) animals were each divided and matched on echocardiography parameters before being semi-randomly assigned to receive the D6D inhibitor (SC) or no drug for 4 weeks. The effect of the D6D inhibition was also examined in 3 month old SHHF rats exposed to a sham TAC surgery (Sham) that were followed along with TAC groups for 4 weeks as an experimental control. All animals were provided Purina 5001 chow and water ad libitum for the duration of the study. At the conclusion of the study, animals were sacrificed with a lethal dose of sodium pentobarbital (150 mg/kg i.p.) followed by midline thoracotomy and removal of the heart. All procedures were approved by the Animal Care and Use Committee at Colorado State University and/or University of Colorado Boulder in strict compliance with the *Guide for the Care and Use of Laboratory Animals* published by the US National Institutes of Health (NIH Publication No. 85-23, revised 1996).

Inhibition of D6D in vivo

Rats were administered the potent, orally active D6D inhibitor SC-26196 (a gift from Dr. Mark Obukowicz, Pfizer Corporation), at a dose previously reported to selectively inhibit D6D enzyme activity with no effect on other desaturase enzymes in rodents *in vivo* (100 mg/kg/d mixed in chow for 4-weeks), based on daily food consumption records taken over 3-4 weeks prior to treatment [17].

Echocardiography and Blood Pressure

Transthoracic echocardiography was performed under light isoflurane anesthesia prior to and following the 4-week experimental period using a 12 MHz pediatric transducer connected to a Hewlett Packard Sonos 5500 Ultrasound as previously described [49]. Tail cuff blood pressure measurements were obtained in the Sham and HF groups using the Kent Coda 6 system (Kent Scientific, Torrington, CT) in lightly isoflurane-anesthetized rats.

Lipid analyses

Briefly, phospholipids were extracted by thin layer chromatography (total) or liquid chromatography (individual species) for compositional analysis by gas chromatography (fatty acid composition) or electrospray ionization mass spectrometry (cardiolipin molecular species) [44]. Myocardial contents of free AA and eicosanoid species were quantified in lipid extracts obtained from 50 mg of LV tissue by LC/MS/MS methods using deuterated standards as previously described [50].

Mitochondrial isolation and respiratory function

Mitochondria were freshly isolated from ~300 mg of left ventricular (LV) tissue by differential centrifugation in the presence of a protease and assayed for respiratory function using a Clark-type electrode system (Strathkelvin) with pyruvate + malate or palmitoylecarnitine + malate as substrates as previously described [49].

Biochemical analyses

Immunoblotting was performed by standard methods using commercially available antibodies. Serum glucose and free fatty acids were determined by colorimetric assays (Biovision). Caspase activities were determined in 30 mg of LV homogenates by luminescence assay (Promega). Myocardial hydroxyproline was quantitated as a marker of collagen (fibrosis) in 30-40 mg of septal tissue by the colorimetric assay of Switzer and Summer [51]. Serum cytokines were determined in 80 μ L of sample by ELISA cytokine array (Raybiotech). qRT-PCR was performed using 2X SYBR Green qPCR Master Mix and validated gene specific primers (listed in Table S2) with resulting data normalized to 18S rRNA and analyzed according to the comparative ($\Delta\Delta$ Ct) Ct method.

Statistical analyses

All data are presented as group means \pm standard error. Human heart data were compared by one-way ANOVA with Tukey tests *post hoc* when appropriate. Rat data were analyzed by 3(condition) X 2(drug) ANOVA to determine main and interaction effects with Tukey tests *post hoc* for determination of significant group differences. Within-group differences in

echocardiography data from pre- to post-treatment were compared by paired t-tests. Statistical significance was established at $P < 0.05$ for all analyses.

Results

Animal characteristics and circulating cytokines

No significant effects of D6D inhibition were observed on body weight, serum glucose, free fatty acids, or blood pressure in any of the groups (Table 3.1). However, significant elevations in serum interferon-gamma (IFN γ) and serum monocyte chemoattractant protein-1 (MCP-1) in TAC and HF groups were attenuated with SC-26196 treatment, consistent with an anti-inflammatory effect of D6D inhibition [17].

Phospholipid indices of D6D activity are elevated in the failing human heart and are reversed by mechanical unloading

Reduced levels of cardiolipin molecular species normally enriched with LA acyl-chains have been reported in hearts explanted from patients with dilated and ischemic cardiomyopathies [42] [16]. However, whether these changes occur in other phospholipid classes or are reflective of a global redistribution of PUFAs in the total myocardial phospholipid pool was not addressed. Compositional analysis of myocardial phospholipids was performed from age-matched individuals with no cardiac pathology (NF; n = 8) and from patients with dilated cardiomyopathy (DCM; n = 8) with or without mechanical unloading with a left ventricular assist device for at least 4 month prior to explanation (LVAD; n = 4) (Fig 3.1). Hearts from patients with dilated cardiomyopathy demonstrated a marked decrease in total phospholipid LA, with corresponding increases in AA, DHA and PUFA product/precursor ratios reflective of D6D hyperactivity

compared to donor hearts from NF. LVAD significantly increased phospholipid LA levels while reducing levels of AA, DHA and D6D product/precursor ratios compared to DCM.

D6D inhibition reverses phospholipid PUFA remodeling in TAC and HF and normalizes the cardiolipin molecular species profile in mitochondria

As was seen in the hearts from DCM patients, hearts from TAC and HF rats also demonstrated marked decreases in LA, with parallel increases in AA, DHA, and D6D product/precursor ratio in total myocardial phospholipids compared to Sham controls (Fig 3.2A). Strikingly, chronic administration of the D6D inhibitor ameliorated these effects in both TAC and HF, seen as total myocardial phospholipid LA, AA, and DHA and D6D activity indices returning near to Sham control levels (Fig 3.2B).

Alterations in the highly regulated fatty acid composition of cardiolipin may have particular relevance in cardiac pathologies [15]. Therefore, cardiolipin molecular species were also examined in cardiac mitochondria isolated from animals in this study. As previously reported [16], a marked loss of the predominant tetra-linoleoyl species (L₄CL) was seen in TAC and HF mitochondria, which corresponded to elevations in species containing AA and/or DHA (highly unsaturated CL; HUFA(CL)), without any appreciable effect on total CL content (Fig 3.2C). D6D inhibition completely normalized the CL molecular species profile in TAC and HF, restoring L₄CL and reducing HUFA(CL) species to Sham control levels in both groups.

Myocardial free arachidonic acid and eicosanoid contents

Once liberated from phospholipids by phospholipase enzymes, AA can serve as a precursor for several bioactive eicosanoid species with complex effects on inflammatory,

cardiovascular and transcriptional regulation [31, 32]. Both TAC and HF elicited significant increases in free AA and several eicosanoid species in the heart, all of which were reduced to near control levels with D6D inhibition (Fig 3.2D). Particularly significant changes were seen in 12- and 15-hydroxyeicosatetraenoic acid (12- and 15-HETE), thromboxane A₂ (TXA₂), and isoprostanes (IPs), which are formed via 12/15-LO, COX-2, and the non-enzymatic peroxidation of AA by ROS, respectively.

D6D inhibition attenuates maladaptive cardiac remodeling and contractile dysfunction

Echocardiography performed before and after the 4-week experimental period revealed significant progression of left ventricular dilatation and contractile dysfunction in the untreated TAC and HF animals that were significantly attenuated or reversed by D6D inhibition (Fig 3.3A, B). These improvements corresponded to lower final heart and lung weights in the treated compared to untreated animals (Fig 3.3C). Myocardial fibrosis, assessed by tissue hydroxyproline content, was also reduced by D6D inhibition in both TAC and HF, which paralleled histological evidence of reduced interstitial and perivascular collagen deposition (Fig 3.4A, B). TAC and HF significantly increased mRNA expression of atrial natriuretic peptide (ANP) and myocardial extracellular-regulated activated kinase 1/2 (ERK1/2) phosphorylation compared to Sham controls, which was largely prevented by D6D inhibition in both models (Fig 3.4C, D). TAC, and to a lesser extent, HF, were both associated with myocardial activation of nuclear factor kappa B (NFκB), indicated by degradation of its endogenous inhibitory regulator I kappa B alpha (IκBα), which was significantly attenuated with D6D inhibition in TAC, but not HF (Fig 3.4E).

Cardiac mitochondrial respiration and caspase activities

Reduced capacity and/or efficiency of oxidative phosphorylation in cardiac mitochondria may impair myocardial bioenergetics and contribute the development and/or progression of heart failure [40]. However, in the presence of pyruvate + malate, TAC had no effect on SSM state 3 (ADP phosphorylating) or state 4 (uncoupled) respiration in the absence or presence of D6D inhibition (Fig 3.5A). Conversely, HF SSL was associated with depressed state 3 respiration and respiratory control (RCR) compared to TAC and Sham. D6D inhibition decreased state 4 respiration and restored RCR to near Sham control levels in HF SSL, but had no effect on state 3 respiration. Restoration of LA-enriched cardiolipin with D6D inhibition in HF IFM had no effect on these three parameters (Fig 3.5B). Furthermore, in the presence of palmitoylcarnitine + malate, D6D inhibition in HF decreased state 4 respiration only in IFM while RCR was decreased in both SSL and IFM while having no effect in on state 3 respiration (Fig 3.5C).

Immunoblotting of mitochondrial proteins for respiratory complex subunits revealed a deficiency in complexes I and II in HF, which is consistent with reduced respiratory capacity in this group (Fig 3.5D), but this was similarly unaffected by D6D inhibition. Activities of caspase-9 and caspase-3/7 were elevated in myocardial tissue from TAC and HF rats compared to Sham controls (Fig 3.5E). Treatment with SC-26196 significantly attenuated caspase activities in TAC, but had no effect in HF.

D6D inhibition reduces cardiac lipoxidative stress

Aldehyde products of PUFA peroxidation such as malondialdehyde (MDA) and 4-hydroxynonenal (HNE) are common markers of oxidative stress that correlate closely with the incidence and severity of heart failure in humans [52]. The peroxidizability of PUFAs increases

exponentially with their double bond content [10]; therefore, the calculated cardiac membrane peroxidizability index increased significantly in TAC and HF, and was normalized to Sham levels by D6D inhibition (Fig 3.6A). Consistent with this observation, MDA- and HNE-protein adducts were elevated in TAC and HF hearts, and were significantly reduced by D6D inhibition (Fig 3.6B). Myocardial MDA levels correlated positively with the relative proportion of DHA in myocardial phospholipids across the experimental groups, whereas a strong negative correlation was seen between HNE and phospholipid LA (Fig 3.6C). D6D inhibition also tended to decrease myocardial superoxide dismutase (SOD) and glutathione peroxidase (GSHPx) enzyme contents (Fig 3.6D), collectively suggesting a decrease in myocardial oxidative stress.

Cardiac and hepatic D6D expression

While our lipid analyses support a central role of D6D in myocardial phospholipid remodeling associated with pressure overload, the mechanism driving D6D activity in response to hemodynamic stress is less clear. D6D expression in the heart is very low, and while detectable, we found no evidence of upregulation at the mRNA or protein level, or any significant changes in expression of downstream elongation/desaturation enzymes in TAC, HF or human DCM (Fig 3.7). Little is known regarding posttranslational regulation of D6D activity, but putative mechanisms are currently being investigated in our laboratory.

Discussion

The present study demonstrates a pivotal role of essential fatty acid metabolism through D6D in generating the signature pattern of phospholipid PUFA redistribution associated with cardiac pathology in multiple experimental models, and show that it is closely linked to

hemodynamic stress in the failing human heart. The remarkable phenotypic effects of D6D inhibition in TAC and HF animals highlight the pathophysiological importance of this process, and provide novel insight into the mechanisms responsible for maladaptive remodeling and contractile dysfunction in the pressure overloaded myocardium.

The proportional loss of phospholipid LA with the corresponding increase in long-chain PUFAs is the most marked and consistent manifestation of membrane remodeling associated with cardiac overload across species, tissues, and phospholipid classes observed herein and in previous studies. Cardiolipin is a dimeric tetra-acyl phospholipid found exclusively in mitochondria, where it provides critical structural and functional support to proteins involved in oxidative phosphorylation, and regulates apoptotic signaling by binding cytochrome c to the inner mitochondrial membrane [15, 53]. The majority of cardiolipin molecular species in the healthy mammalian heart contain four LA acyl chains (L_4CL). Several studies report that this LA enrichment is lost in states of cardiac pathology, which has been suggested as a potential contributor to mitochondrial dysfunction and disease progression [15]. It is well established that the compositional uniformity of cardiolipin results from a series of deacylation and reacylation reactions following *de novo* biosynthesis in mitochondria. Our data demonstrate that changes in cardiolipin composition coincide with changes in PC, PE and total phospholipid fractions reflective of a global redistribution of membrane PUFAs in the heart. This ultimately reduces the bioavailability of phospholipid LA for cardiolipin remodeling in the heart, favoring an exchange of LA for long-chain PUFA products, such as AA and DHA, of this pathway.

Reduced capacity and/or efficiency of oxidative phosphorylation in cardiac mitochondria may contribute to the development and/or progression of heart failure, and aberrant cardiolipin remodeling has been postulated as a mechanism for these defects [16, 49]. However, despite a

significant loss of L₄CL, TAC had no effect on mitochondrial respiratory function in the absence or presence of D6D inhibition. Impaired oxidative phosphorylation capacity was seen in HF mitochondria, but this was unaffected by D6D inhibition and may have resulted from the loss of complexes I and II, which deliver reducing equivalents to the respiratory chain. Reductions in oxidative phosphorylation efficiency may also contribute to cardiac dysfunction in heart failure [54]. Therefore, increases in RCR with D6D inhibition, while relatively modest, could have contributed to improvements in cardiac function observed in HF. Taken together, these findings indicate that the LA enrichment of cardiolipin, at least within the range observed in these studies, does not significantly influence the oxidative phosphorylation capacity of cardiac mitochondria, but may support efficient respiratory coupling.

Cleavage of arachidonic acid from myocardial phospholipids by PLA₂ enzymes for subsequent metabolism as “free” AA by cyclooxygenase (COX), lipoxygenase (LO), or cytochrome P450 monooxygenase enzymes [31], can generate a host of eicosanoid species with diverse biological effects [32]. Myocardial PLA₂ activity is elevated in states of pathologic stress, including heart failure [55], and upregulation of myocardial COX [33] and 12/15-LO [34, 56] pathways have been implicated in the pathogenesis of cardiomyopathy. Therefore, D6D-dependent increases in myocardial levels of free AA and its eicosanoid derivatives observed in TAC and HF animals may have contributed the progression of maladaptive remodeling.

Furthermore, myocardial AA can also promote extracellular receptor kinase (ERK) signaling and cardiac hypertrophy via activation of specific intracellular G protein-coupled receptors by TXA₂ in cardiomyocytes [35, 36]. Overproduction of 12-HETE also increases ERK activity, hypertrophy and fibronectin content in cardiac fibroblasts [56]. Therefore, D6D inhibition might have attenuated maladaptive remodeling by reducing ERK signaling.

Cardiomyocyte NFκB signaling has been implicated in the pathogenesis of cardiac hypertrophy and failure [57]. D6D inhibition tended to attenuate NFκB activation in TAC in the present study, but had no effect in HF. This is consistent with clinical evidence for a greater degree of inflammation associated with compensatory hypertrophy during early aortic stenosis compared to decompensated HF [58].

Apoptotic loss of cardiomyocytes during maladaptive cardiac remodeling may hasten the progression of pathologic hypertrophy to decompensated failure [41]. Myocardial activities of caspase-9 and caspase-3/7 were elevated in both TAC and HF, but were only attenuated by D6D inhibition in TAC. This model-specific effect parallels the pattern of myocardial NFκB activation seen in these animals. This is consistent with evidence linking NFκB activity and apoptotic signaling in the pressure overloaded failing heart [59]. However, the extent to which caspase activities reflect cumulative apoptotic myocyte loss that contributed to the observed changes in cardiac structure and function is unclear.

Membrane PUFAs are a primary target of ROS, which react with hydrogens in methylene groups adjacent to their double bonds, triggering an autocatalytic series of oxidation events leading to chain breaks and reactive aldehyde formation. The susceptibility of PUFAs to peroxidation increases exponentially with double bond content [10]; therefore, modification of membrane PUFA composition could influence the extent of aldehyde formation in states of oxidative stress. Consistent with this hypothesis, D6D inhibition significantly attenuated increases in myocardial MDA- and HNE-protein adducts in TAC and HF, which correlated closely with changes in phospholipid DHA and LA levels, respectively.

The present study reveals a central role of essential fatty acid metabolism through D6D in generating the signature pattern of PUFA redistribution in myocardial phospholipids widely

reported in cardiac pathologies, and it suggests the important pathophysiological implications of such phospholipid remodeling in the heart. Mitochondrial data demonstrate that fatty acid composition of cardiolipin does not have a significant effect on oxidative phosphorylation capacity but perhaps may play a role in coupling in heart failure. Therefore, similar to the findings in the aged mouse, this finding further recapitulates the idea that the alterations in fatty acyl chains of cardiolipin, resulting in the loss of tetra-linoleoyl CL, does not have an independent effect on mitochondrial respiratory function. Moreover, it appears that the main pathogenic effect of this phospholipid remodeling process is an increase in myocardial free AA, favoring production of multiple eicosanoid species implicated in hypertrophic and fibrotic remodeling.

Table 3.1. Animal Characteristics and Serum Analyses

	Sham	Sham+SC	TAC	TAC+SC	HF	HF+SC
Body Weight, g	285 ± 8	289 ± 10	260 ± 8	259 ± 10	394 ± 10	381 ± 11
Systolic BP, mmHg	151 ± 10	153 ± 11	ND	ND	175 ± 15	188 ± 11
<i>Serum Analyses</i>						
Glucose, mM	6.2 ± 0.9	6.1 ± 0.3	6.6 ± 0.5	6.8 ± 1.1	6.8 ± 0.5	5.5 ± 3
FFA, μM	314 ± 15	306 ± 20	308 ± 28	287 ± 25	283 ± 13	296 ± 25
IFNg, pg/mL	28 ± 18	ND	89 ± 9*	51 ± 15†	135 ± 12*	87 ± 19*†
IL-1β, pg/mL	107 ± 50	ND	161 ± 15*	163 ± 47	152 ± 50	92 ± 21
IL-10, pg/mL	549 ± 289	ND	241 ± 41*	337 ± 41	309 ± 45	430 ± 49
MCP-1, pg/mL	1143 ± 645	ND	2267 ± 285*	1573 ± 261†	2175 ± 151*	1674 ± 241†
TIMP-1, pg/mL	4405 ± 1745	ND	4436 ± 437	5086 ± 473	4773 ± 418	5122 ± 680

Data are means ± SEM. Abbreviations: BP, blood pressure; FFA, free fatty acids; IFNg, interferon gamma. IL, interleukin; MCP-1, macrophage chemotactic protein-1 TIMP-1, TIMP metalloproteinase. * $P < 0.05$ vs. Sham; † $P < 0.05$ vs. untreated.

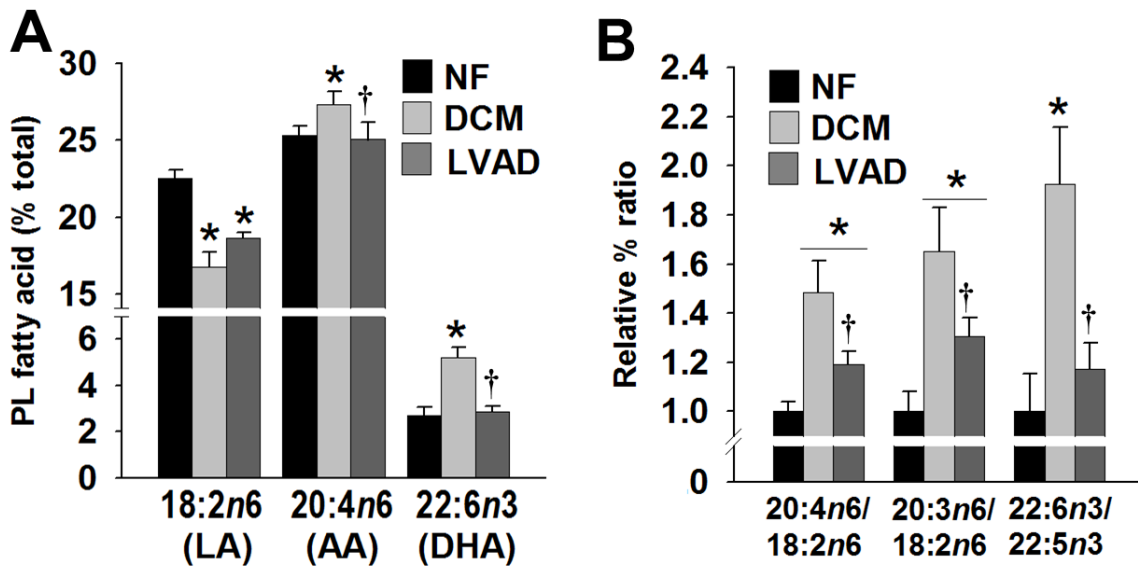


Figure 3.1. Phospholipid PUFA desaturation in human heart failure

Gas chromatographic analysis of total phospholipid fatty acids extracted from human left ventricular tissue revealed a loss of phospholipid LA paralleled by elevations in AA, DHA and PUFA product/precursor ratios in hearts explanted from patients with dilated cardiomyopathy (DCM; n = 8) compared to non-failing donor hearts (NF; n = 8), which was partially reversed in patients implanted with a left ventricular assist device for 4-10 months (LVAD; n = 4). * P < 0.05 vs. NF. † P < 0.05 vs. DCM.

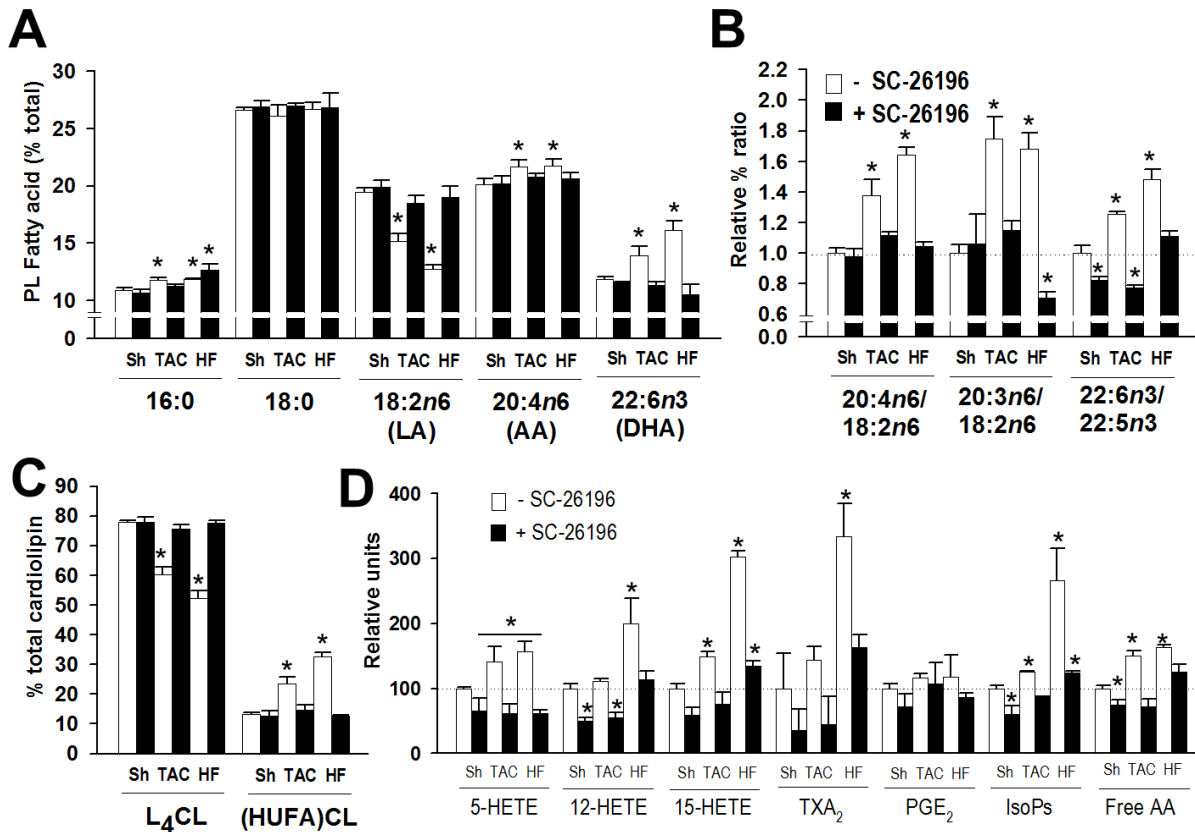


Figure 3.2. Myocardial phospholipid composition and eicosanoids

Treatment of TAC and HF animals with the selective D6D inhibitor SC-26196 for 4 weeks (black bars) normalized relative proportions of LA, AA and DHA (A), and reversed D6D product/precursor indices (B) in the global myocardial phospholipid pool (n= 8-10/group). C) Mass spectrometry of cardiolipin molecular species revealed a restoration of L₄CL and CL species containing highly unsaturated fatty acids (HUFAs) to control levels in cardiac mitochondria with D6D inhibition (n = 4-6/group). D) SC-26196 treatment significantly attenuated elevations in myocardial unesterified (“free”) AA and several of its pathogenic eicosanoid derivatives (n = 4-6/group). A significant group X drug interaction effect was seen for all analyses except 16:0, 18:0, and PGE₂, therefore only significant group differences vs. Sham control at $P < 0.05$ (*) are indicated for clarity. See text for abbreviations.

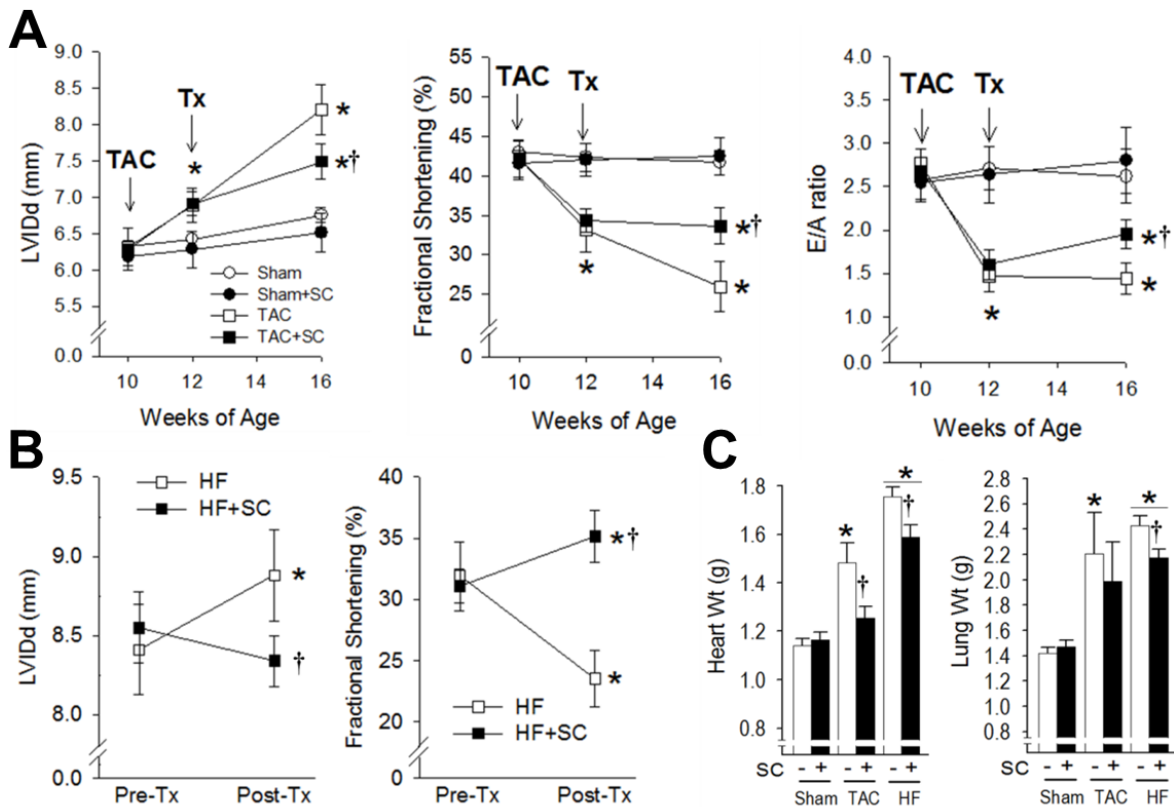


Figure 3.3. D6D inhibition attenuates contractile dysfunction and pathologic hypertrophy in TAC and HF

Serial echocardiography revealed marked left ventricular dilatation (LV internal diameter in diastole; LVIDd), systolic dysfunction (decreased fractional shortening) and diastolic dysfunction (decreased E/A ratio) in TAC animals (n=8), which was significantly attenuated by D6D inhibition (SC; n=8) beginning 2 weeks following surgery (Tx) (A). LV dilatation and systolic dysfunction in aged SHHF rats (n = 12) during the 4-week experimental period was attenuated or reversed by D6D inhibition (n = 10) (B). SC treatment resulted in significantly lower heart weights in TAC and HF animals, and decreased pulmonary congestion in HF rats (C). * P < 0.05 vs. Sham or Pre-Tx HF. † P < 0.05 vs. untreated.

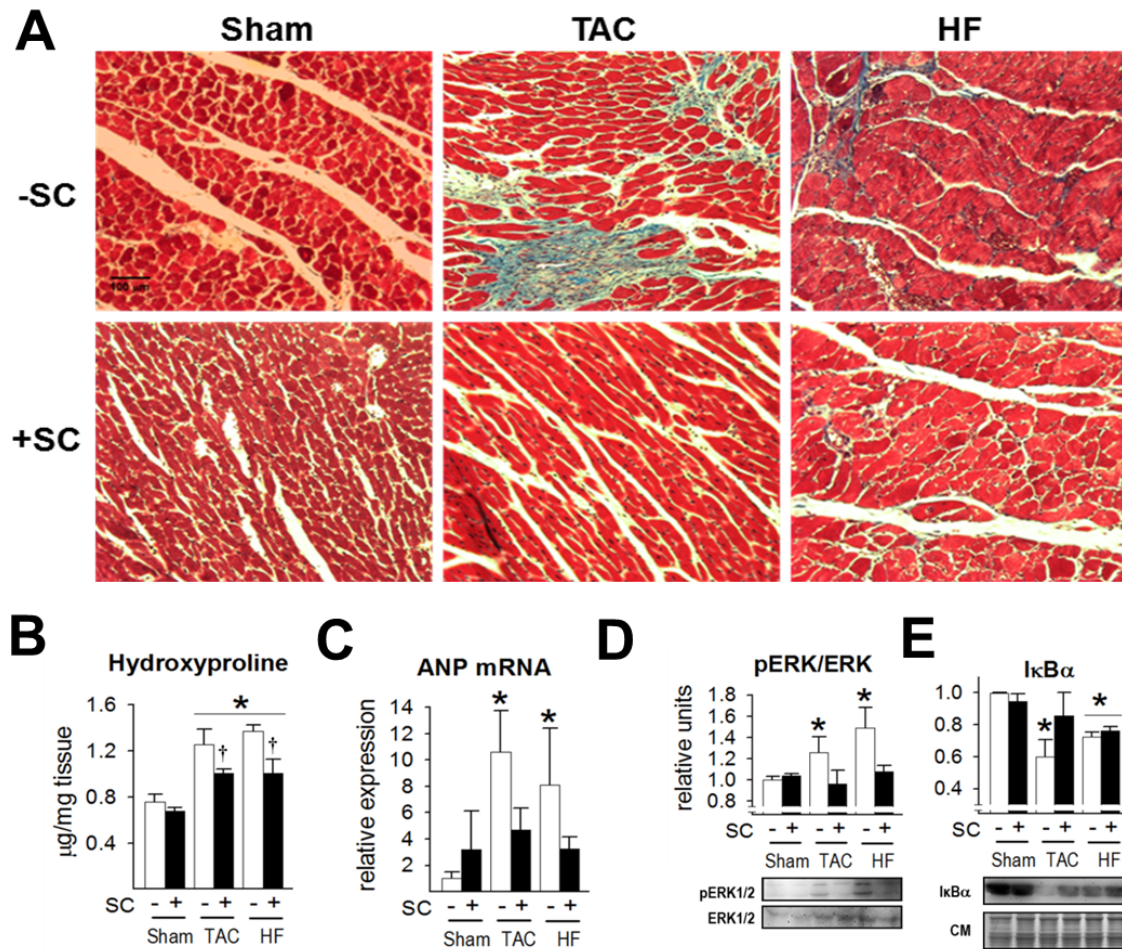


Figure 3.4. Myocardial fibrosis, hypertrophic and inflammatory signaling

Masson's trichrome staining of LV tissue from TAC and HF animals revealed interstitial and perivascular fibrosis that was markedly reduced with D6D inhibition (A), which paralleled a significant attenuation of elevated myocardial hydroxyproline (collagen) content in TAC and HF animals ($n = 6/\text{group}$) (B). SC treatment prevented significant elevations in ANP expression (C) and ERK phosphorylation (D) in TAC and HF, and attenuated loss of the endogenous NF κ B inhibitor I κ B α (E) in TAC ($n = 4-6/\text{group}$). * $P < 0.05$ vs. Sham or Pre-Tx HF. † $P < 0.05$ vs. untreated.

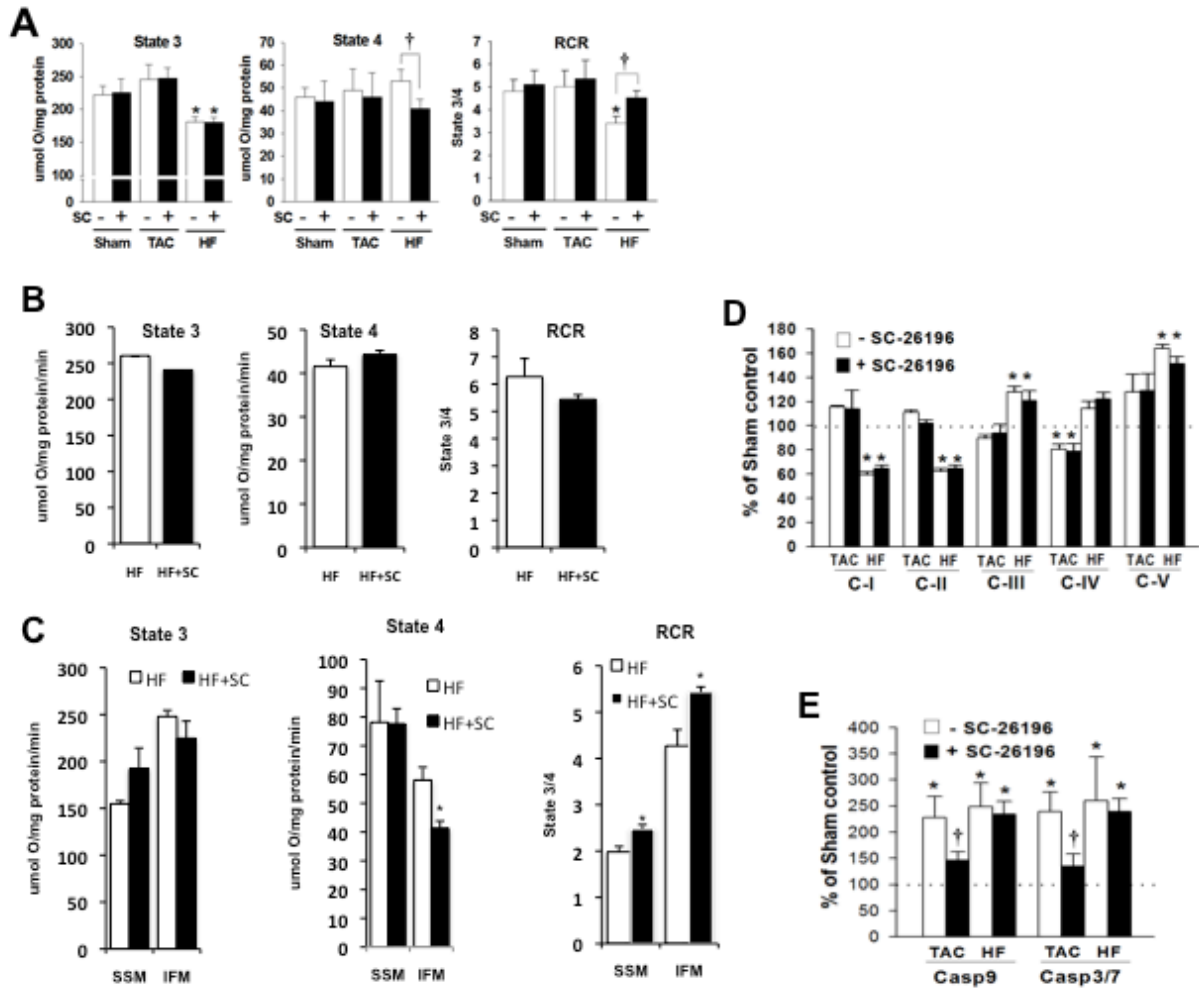


Figure 3.5. Mitochondrial respiration and caspase activities

A) State 3 (phosphorylating) and State 4 (uncoupled) respiration, respiratory control ratio (RCR, state3/4) in cardiac SSL in the presence of pyruvate + malate (n =4-8/group). B) State 3 (phosphorylating) and State 4 (uncoupled) respiration, respiratory control ratio (RCR, state3/4) in cardiac IFM in the presence of pyruvate + malate (n =4-8/group). C) State 3 (phosphorylating) and State 4 (uncoupled) respiration, respiratory control ratio (RCR, state3/4) in cardiac SSL and IFM in the presence of palmitoylecarnitine + malate (n =4-8/group). D) Protein expression of subunits from each of the five respiratory complexes (CI-V) obtained by immunoblotting 10ug of mitochondrial protein (n = 4/group). E) Caspase activities in myocardial homogenates assayed by luminescence assay (n = 4-6/group). * P < 0.05 vs. Sham control. † P < 0.05 vs. untreated.

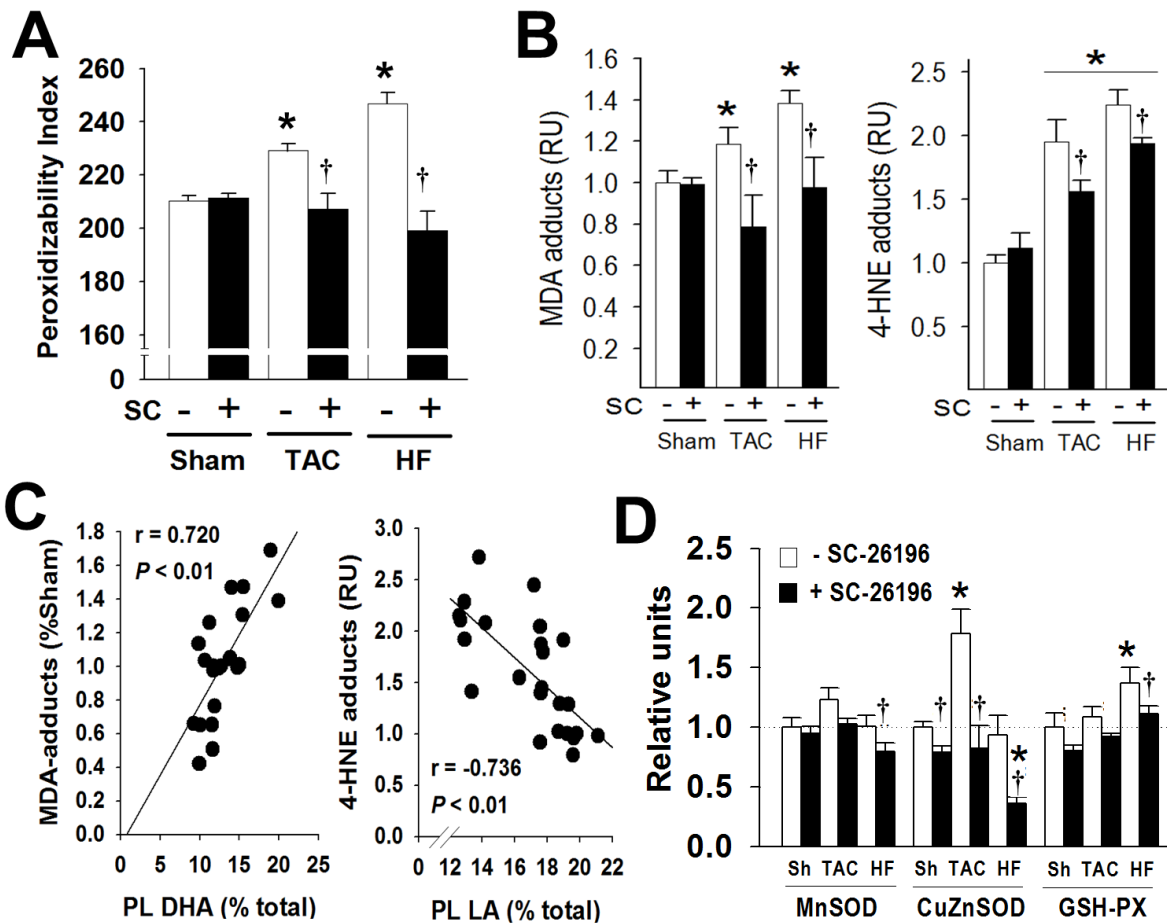


Figure 3.6. Myocardial lipoxidative stress

A) Membrane peroxidizability index of total myocardial phospholipids calculated from fatty acid analyses in Figure S1 as: (%monoenoic X 0.025)+ (%dienoic X 1)+(%trienoic X 2)+(%tetraenoic X 4)+(%pentaenoic X 6)+(%hexaenoic X 8). B) Relative contents of malondialdehyde (MDA) and 4-hydroxynonenal (4-HNE) protein adducts in myocardial homogenates (n = 4-6/group). C) Scatterplots of data from tissue for which both total phospholipid fatty acid profiles and lipid aldehyde-adduct data reveal significant correlations between MDA and membrane DHA, and between 4-HNE and LA. D) Myocardial contents of Mn and Cu/Zn superoxide dismutase (SOD) isozymes and glutathione peroxidase (GSHPx) (n = 4-6/group). * P < 0.05 vs. Sham control. † P < 0.05 vs. untreated. A significant main effect of D6D inhibition was seen in all three enzymes by ANOVA (P < 0.05).

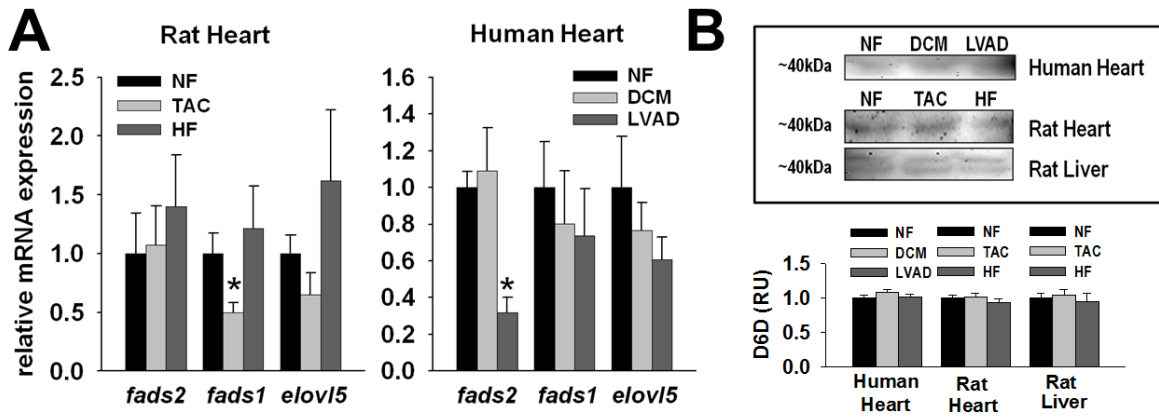


Figure 3.7. D6D pathway expression

(A) Relative mean (+/- SEM) data for qRT-PCR of mRNA encoding D6D (*fads2*), delta-5 destaurase (*fads1*), and elongase-5 (*elov15*) in the rat and human heart. *P < 0.05 vs. NF; n = 4-6/group. (B) Representative blots and mean (+/- SEM) data for D6D protein by immunoblotting in rat and human tissues (n = 6/group).

Cardiac Mitochondrial Phenotype of the *Taz* shRNA Mouse Model of Human Barth Syndrome³

Summary

Barth syndrome (BTHS) is an X-linked cardioskeletal myopathy resulting from a mutation in the Tafazzin (*TAZ*) gene encoding a mitochondrial transacylase required for the remodeling of cardiolipin (CL). CL is an inner membrane phospholipid essential for the function of several mitochondrial proteins, but it remains unclear how *Taz* deficiency or aberrant CL remodeling lead to mitochondrial dysfunction and cardiomyopathy. In this study, the cardiac mitochondrial phenotype of a new *Taz* shRNA mouse model of BTHS was characterized. High-resolution respirometry revealed 40-50% lower OXPHOS rates in *Taz* versus wild-type (WT) mitochondria using pyruvate and palmitoylcarnitine (PalmCrtn) as substrates (P < 0.001). Succinate respiration was also lower in *Taz*, but only by 13% (P = 0.07), suggesting a possible defect in Complex 1 and/or NADH generation from pyruvate and Pal oxidation. Interestingly, glutamate respiration was 46% greater in *Taz* vs. WT (P < 0.05), and reached OXPHOS rates equal to that obtained with pyruvate and PalmCrtn in WT mitochondria. Analysis of the *Taz* mitochondrial proteome revealed deficiencies in enzymes involved in beta-oxidation, pyruvate transport, amino acid catabolism, complex I, and the TCA cycle. However, malate

³Catherine H. Le^{*}, Anthony B. deMooy[#], Christopher M. Mulligan⁺, Adam L. Heuberger[◇],
Jessica E. Prenni[◇], Adam J. Chicco^{*+##†}

^{*}Cell and Molecular Biology Program, Departments of[#]Biomedical Sciences, ⁺Food Science and Human Nutrition, [†]Health and Exercise Science, [◇]Biochemistry and Molecular Biology, Colorado State University, Fort Collins, CO, USA

dehydrogenase, the primary source of NADH from glutamate oxidation, was elevated 40% in *Taz* versus WT mice ($P < 0.05$). Cardiac metabolomic profiling revealed an accumulation of substrates congruent with observed mitochondrial enzyme deficiencies. Mitochondrial ROS release was reduced in *Taz* versus WT mitochondria. Taken together, these data suggest that *Taz* deficiency selectively impairs carbohydrate and lipid oxidation and propose that perhaps it is the impairment of the tafazzin-mediated CL remodeling process itself, not the resulting change in cardiolipin composition, which causes the mitochondrial respiratory dysfunction in Barth syndrome.

Introduction

Previous data from chapter III demonstrated aberrant cardiolipin remodeling in the failing heart, seen as a loss of linoleic acid with corresponding increases in long-chain highly unsaturated fatty acids. Reversal of this phenomenon reduced myocardial hypertrophy and preserved contractile function. However, similar to the findings in the aged heart presented in chapter II, restoration of cardiolipin composition in the failing heart also did not have a significant effect on mitochondrial respiratory function, further dissociating changes in cardiolipin composition from cardiac mitochondrial respiratory dysfunction in these conditions. This disconnect is intriguing because Barth syndrome, classified as a mitochondrial disease, is characterized by a signature loss of LA enrichment in cardiolipin. This multisystem disease results in childhood-onset dilated cardiomyopathy, exercise intolerance, growth retardation, and neutropenia, underscoring the biological importance of cardiolipin in human health.

Barth syndrome (BTHS; 3-methylglutaconic aciduria type II) is an X-linked mitochondrial disorder that results from mutations in the tafazzin gene (*Taz*), leading to symptoms reflective of impaired bioenergetics. While the precise pathogenic mechanisms of

disease are unclear, it is known that the tafazzin gene is mutated in BTHS [60-63]. *Taz* encodes a phospholipid transacylase required for the remodeling of cardiolipin (CL), where it functions to transfer acyl groups from adjacent phospholipids such as phosphatidylcholine (PC) to cardiolipin. In a recent paper by Schlame et al., it was demonstrated that the resulting acyl specificity of CL arises not on the basis of intrinsic function of tafazzin but instead as a result of the bioavailability and physical properties of the lipids. Interestingly, the study also demonstrated tetralinoleoyl-cardiolipin forms only under conditions which favored the hexagonal phase [64].

The presence of CL is essential for maintaining the structural and functional integrity of mitochondria, including the assembly and enzymatic activity of electron transport system (ETS) complexes [65-68]. In the healthy mammalian heart, 80-90% of CL acyl chains are linoleic acid (18:2n6), and tetra-linoleoyl CL (18:2₄ CL) accounts for the vast majority of molecular species. Linoleoyl enrichment of CL is achieved by a complex series of acyl chain exchange reactions with adjacent monomeric phospholipids catalyzed by *Taz* following *de novo* biosynthesis in the inner mitochondrial membrane [15, 69-71]. While the precise acyl chain composition of CL varies across different tissues and species, its acyl chain remodeling and molecular symmetry are highly conserved, suggesting an important role in its biological function.

Taz mutations associated with BTHS result in CL deficiency with a marked loss of linoleoyl enrichment and accumulation of monolyso-cardiolipin (MLCL) species [72-74]. These abnormalities have been associated with decreased mitochondrial respiratory enzyme function, increased production of reactive oxygen species (ROS), and/or impaired mitochondrial protein sorting and import in BTHS cell lines, and *Taz* deficient yeast, *Drosophila*, and zebrafish models [75-79]. While these studies have been valuable in defining putative roles of *Taz* and CL remodeling in mitochondrial function, elucidating the precise mechanism by which *Taz*

dysfunction alters mitochondrial function in cardiac muscle, a primary locus of pathology in BTHS, requires use of a mammalian model.

Genetic ablation of *Taz* in mice results in embryonic lethality; therefore, an inducible *Taz* shRNA knockdown mouse model was recently generated. Initial characterization of this model revealed expected alterations in the cardiac cardiolipin profile, abnormalities in mitochondrial morphology, and cardiac and skeletal muscle dysfunction [80, 81]. Additionally, even though *Taz* deficiency leads to abnormal CL, which has been coupled to mitochondrial respiratory dysfunction, increased ROS production, and initiation of apoptotic signaling, the mechanism of disease in BTHS remains unknown. However, no examination of mitochondrial function has been described in *Taz*-deficient mammalian heart. Consequently, we sought out to characterize the cardiac mitochondrial phenotype of *Taz* deficient mice through a comprehensive integration of functional studies with cardiac metabolomic and mitochondrial proteomic profiling.

Experimental Procedures

Animal model and diet

Six *Taz* shRNA positive founder mice were obtained from Dr. Zaza Khuchua (at CCHMC), which were originally generated at TaconicArtemis, GmbH (Köln, Germany) under contract from the Barth Syndrome Foundation; sequentially, a colony of Barth mice was started and maintained. 200 ppm doxycycline (DOX) was administered as part of the food by Purina Mills (Gray Summit, MO) ad libitum until 2-4 months of age, when animals were anesthetized with sodium pentobarbital and killed by exsanguination via excision of the heart. Mice were genotyped by PCR analysis of tail DNA with previously described sequences [81]. All procedures in this investigation were approved by the Colorado State University Care and Use

Committee and conform to the *Guide for the Care and Use of Laboratory Animals* published by the U.S. National Institutes of Health (NIH Publication No. 85-23, revised 1996).

Mitochondrial isolation

Briefly, mitochondria were freshly isolated from ~200mg of heart tissue (2 hearts pooled) in cold Chappell-Perry buffer consisting of (in mM) KCL (100), MOPS (50), EGTA (1), EGTA (5), MgSO₄·7H₂O (5), and ATP (1), pH 7.4 (with KOH) by standard differential centrifugation methods as previously described with minor modifications [82]. Both subsarcolemmal (SSM) and intermyofibrillar (IFM) subpopulations of mitochondria were isolated, using trypsin to dissociate IFM from myofibrillar proteins.

Fatty acid composition of mitochondrial phospholipids

Initial characterization of *Taz* shRNA mice demonstrated an expected loss of 18:2₄ CL and accumulation of MLCL and CL molecular species containing saturated acyl chains consistent with a lack of cardiolipin remodeling following *de novo* biosynthesis [83, 84]. However, the effect of *Taz* deficiency on the relative proportions of fatty acids in present in mitochondrial phospholipids has not been described. Therefore, a detailed fatty acid compositional analysis of total mitochondrial phospholipids, cardiolipin, phosphatidylcholine (PC), and phosphatidylethanolamine (PE) was performed in lipids extracted from SSM and IFM. To determine the fatty acid composition of total mitochondrial phospholipids, lipids were extracted from of isolated mitochondria (0.5 mg protein) by incubating isolates in 800 μL methanol with 25 μL sodium methoxide solution for 30 seconds to generate phospholipid fatty acid methyl esters, followed by extraction of fatty acids with hexane for subsequent assessment

of fatty acid composition by gas chromatography (GC). Separation of individual phospholipid classes was performed by normal phase liquid chromatography (Agilent Zorbax Rx-Sil column, 4.6 X 250mm, 5-micron) using a Hexane:Isopropanol:Potassium Acetate mobile phase gradient optimized for separation of PE, PC and cardiolipin by UV detection (206 nm). Fractions were collected based on elution time of known standards, evaporated under a nitrogen stream, and resuspended in hexane, followed by the addition of 14% BF₃-methanol and heating at 100 °C for 30 minutes to obtain methyl esters for GC analysis. GC analysis was performed using an Agilent Technologies DB-225 30m x 0.250mm x 0.25µm column (model 122-2232, J&W Scientific) on an Agilent 6890 Series Gas Chromatographer. The initial temperature of the oven was 120 °C with an initial ramp temperature of 10°C/min for 8 minutes, then 2.5°C/min for 4 minutes and held at 210°C for the remaining 6 minutes for a total run time of 20 min. The inlet split ratio was 15:1 with the column at constant flow and an initial flow, pressure, and velocity at 1.8ml/min, 23.59 psi, and 42 cm/sec, respectively.

GC analysis was performed using an Agilent Technologies DB-225 30m x 0.250mm x 0.25µm column (model 122-2232, J&W Scientific) on an Agilent 6890 Series Gas Chromatographer. The initial temperature of the oven was 120 °C with an initial ramp temperature of 10°C/min for 8 minutes, then 2.5°C/min for 4 minutes and held at 210°C for the remaining 6 minutes for a total run time of 20 min. The inlet split ratio was 15:1 with the column at constant flow and an initial flow, pressure, and velocity at 1.8ml/min, 23.59 psi, and 42 cm/sec, respectively.

Mitochondrial respiration

Oxidative phosphorylation in rates in response to 50µM ADP were determined in freshly

isolated mitochondria (75µg protein) using the two-channel high resolution respirometer (Oroboros Oxygraph; Innsbruck, Austria) with the saturating concentrations of the following substrate combinations (in mM): pyruvate (5) + malate (5), palmitoylcarnitine (0.04) + malate (5), succinate (10) + rotenone (0.0001), or malate (5) + glutamate (10). Respiration studies were performed at an initial oxygen concentration of 150 µM at 37°C in MiR06 respiration buffer containing (in mM) EGTA (0.5), MgCl₂·6 H₂O (3), K-lactobionate (60), taurine (20), KH₂PO₄ (10), HEPES (20), sucrose (110), 1g/L BSA, 280U/ml catalase, pH 7.4 (with KOH).

Complex I and complex IV activities

Complex I and IV activities were determined as previously described in frozen-thawed mitochondrial isolates using standard spectrophotometric methods on the Spectramax M2e spectrofluorometer (Molecular Devices) [44].

Co-A Assay

10µl of isolated mitochondria with concentrations between 10-15mg/ml was used in a commercially available colorimetric assay kit (BioVision; catalog #K367-100). CoA concentration was normalized to mitochondrial protein concentration.

Proteomic Profiling

Protein digestion- 30µg of the isolated mitochondrial proteins were precipitated with acetone, resuspended in 8 M urea and 0.2% ProteaseMAX surfactant (Promega), reduced with dithiothreitol, and alkylated with iodoacetamide. The proteins underwent tryptic digestion for 3 h at 37°C and then stopped with 0.5% trifluoroacetic acid. Peptides were dried in a speed-vac and

purified using a reverse phase C18 TopTip (Glygen). Purified peptides were dried and reconstituted in 50 μ l of 0.1% formic acid/3% acetonitrile. Mass Spectrometry- Peptides were further purified and concentrated using an on-line enrichment column (Agilent Zorbax C18, 5mm, 5 x 0.3mm). Subsequent chromatographic separation was performed on a reverse phase nanospray column (Agilent 1100 nanoHPLC, Zorbax C18, 5mm, 75 mm ID x 150mm column) using a 90 minute linear gradient from 25%-55% buffer B (90% ACN, 0.1% formic acid) at a flow rate of 300 nanoliters/min. Peptides were eluted directly into the mass spectrometer (Thermo Scientific LTQ linear ion trap) and spectra were collected over a m/z range of 200-2000 Da using a dynamic exclusion limit of 3 MS/MS spectra of a given peptide mass for 30 s (exclusion duration of 90 s). Compound lists of the resulting spectra were generated using Xcalibur 2.2 software (Thermo Scientific) with an intensity threshold of 5,000 and 1 scan/group. Data Analysis- MS/MS spectra were searched against the mouse Uniprot protein database (version 02/09/12) concatenated with reverse sequences for determination of the peptide FDR (118,690 sequence entries) using both the Mascot database search engine (version 2.3) and SorcererTM-SEQUEST[®] [85]. Search parameters were as follows: average mass, parent ion mass tolerance of 2 Da, fragment ion mass tolerance of 1.5 Da, fully tryptic peptides with 1 missed cleavage, variable modification of oxidation of M and fixed modification of carbamidomethylation of C. Search results for each independently analyzed sample were imported and combined using probabilistic protein identification algorithms implemented in Scaffold software (Version 3.6.2, Proteome Software, Portland, OR) [86, 87]. Peptide and protein probability thresholds of 95% and 99% respectively, and a minimum of two unique peptides, were applied and resulted in a peptide FDR of 0.1% as calculated by Scaffold based on matches to reverse hits. Proteins containing shared peptides were grouped by Scaffold to satisfy

the laws of parsimony. Manual validation of MS/MS spectra was performed for all protein identifications above the probability thresholds that were based on only two unique peptides. Criteria for manual validation included the following: 1) minimum of 80% coverage of theoretical y or b ions (at least 5 in consecutive order); 2) absence of prominent unassigned peaks greater than 5% of the maximum intensity; and 3) indicative residue specific fragmentation, such as intense ions N-terminal to proline and immediately C-terminal to aspartate and glutamate (used as additional parameters of confirmation.) Relative quantitation was determined by spectral counting (Liu 2004) [88]. Raw spectral counts were normalized in Scaffold by applying a scaling factor such that the total spectral counts for each biological replicate are the same. A student's t-test was applied to calculate p-values. For relative quantitation by spectral counting, the protein list was further filtered by the following criteria: proteins must be present in a minimum of 2 out of 3 biological replicates for a given state and the total normalized spectral counts for a given state must be > 10.

Metabolite extraction and detection by GC-MS

Heart tissue was frozen in liquid nitrogen and ground to a fine powder using mortar and pestle. One mL of methanol/water (70:30) was added to 20 mg of heart tissue and shaken on a vortex mixer for 2 hours. Samples were centrifuged at 3000xg for 10 min at 4 °C, and 800 µL of the supernatant was transferred to a 1.5 mL microcentrifuge tube. The extract was dried using a speedvac, resuspended in 50 µL of pyridine containing 15 mg/mL of methoxyamine hydrochloride, incubated at 60°C for 45 min, sonicated for 10 min, and incubated for an additional 45 min at 60°C. Next, 50 µL of N-methyl-N-trimethylsilyltrifluoroacetamide with 1% trimethylchlorosilane (MSTFA + 1% TMCS, Thermo Scientific) was added and samples were

incubated at 60 °C for 30 min, centrifuged at 3000xg for 5 min, cooled to room temperature, and 80 µL of the supernatant was transferred to a 150 µL glass insert in a GC-MS autosampler vial. Metabolites were detected using a Trace GC Ultra coupled to a Thermo DSQ II (Thermo Scientific). Samples were injected in a 1:10 split ratio twice in discrete randomized blocks. Separation occurred using a 30 m TG-5MS column (Thermo Scientific, 0.25 mm i.d., 0.25 µm film thickness) with a 1.2 mL/min helium gas flow rate, and the program consisted of 80 °C for 30 sec, a ramp of 15 °C per min to 330 °C, and an 8 min hold. Masses between 50-650 m/z were scanned at 5 scans/sec after electron impact ionization. For each sample, a matrix of molecular features as defined by retention time and mass (m/z) was generated using XCMS software [REF1 below]. Features were normalized to total ion current, and the relative quantity of each molecular feature was determined by the mean area of the chromatographic peak among replicate injections (n=2). Molecular features were formed into peak groups using AMDIS software [REF2 below], and spectra were screened in the National Institute for Technology Standards (www.nist.gov) and Golm (<http://gmd.mpimp-golm.mpg.de/>) metabolite databases for identifications. Pantothenic acid was validated by comparing retention times and mass spectra from heart extracts to a commercial standard [89, 90].

Mitochondrial H₂O₂ release

Mitochondrial ROS release was measured as H₂O₂ in freshly isolated mitochondria using the fluorometric Amplex UltraRed probe (Molecular Probes) in the presence of horseradish peroxidase (HRP) as previously described [19]. The concentrations of HRP and Amplex UltraRed in the incubation were 0.12U/ml and 59.1µM, respectively. Fluorescence was measured in a microplate reader (SpectraMax M5; Molecular Devices; Sunnyvale, CA, USA)

with 560 nm excitation and 590 nm emission wavelengths. 30µg of mitochondria were incubated at room temperature in 50mM KH₂PO₄, pH 7.4. H₂O₂ production was monitored under state 4 conditions in the presence of oligomycin (5µg/ml) using succinate (5mM) + rotenone (2.4µM) (SROA; complex 2 linked), malate (5 mM) + pyruvate (5mM) (MPOA; complex 1 linked), succinate (5mM) + rotenone (2.4µM), + antimycin A (10µM) (SROAA; maximal). Background fluorescence was measured in the absence of mitochondria [19].

Mitochondrial oxidative stress

30µg mitochondrial isolate was used to blot HNE-adducts (Calbiochem; catalog #393207; 1:2000 dilution). Briefly, isolated mitochondria were lysed in 2x lysis buffer with protease inhibitor. After sonication, mitochondrial supernatant was resuspended in 2x lammeli buffer, heated for 10 mins at 100C, and then loaded into a polyacrylamide gel. After electrophoresis and transfer, membranes were stained with Ponceau S for internal loading control then blocked in 5% nonfat dry milk (NFM) in TTBS (Tris buffered saline with 1% tween) for 1hr. All primary antibodies were diluted in 1% NFM in TTBS and incubated overnight at 4C. Chemiluminescence was detected with a UVP ChemiDoc imager (UVP; Upland, CA, USA)

Statistical analyses

All data are presented as group means \pm standard error. Statistical significance was established as $P \leq 0.05$ for all analyses.

Results

Animal Characteristics

A total of 58 mice (28 *Taz* and 30 WT) were used in our studies ranging from 3-5 months of age. Body weight was significantly lower in *Taz* (25.8 ± 0.6 g) compared to WT (34.0 ± 1.3 g; $P < 0.01$), consistent with previously reported growth delay and small stature present in this model and BTHS patients [84]. Heart weights were not significantly different between groups (142 ± 9 versus 149 ± 4 mg in *Taz* and WT), however heart/body weight ratios were significantly higher in *Taz* (5.5 ± 0.1 mg/g) versus WT (4.4 ± 0.3 g; $P < 0.01$).

Cardiac mitochondrial phospholipid fatty acid composition

Figure 4.1 illustrates the effect of *Taz* deficiency on the fatty acid composition of SSM and IFM phospholipids. Consistent with mass spectrometry data previously reported [84], *Taz* deficiency elicited a marked loss of 18:2n6 content in cardiolipin paralleled by reciprocal increases in monounsaturated and saturated fatty acids indicative of defective remodeling. Marked elevations in 18:2n6 were seen in mitochondrial PC, but not PE, suggesting that PC may be a primary source of 18:2n6 for cardiolipin transacylation by tafazzin in the mouse heart [71] or may accumulate 18:2n6 to compensate for the lack of 18:2₄CL by another mechanism. Several significant changes in fatty acid composition were seen in total mitochondrial phospholipids in *Taz* vs. WT, including a loss of 18:2n6, an increase in arachidonic acid (20:4n6), and a decrease in docosahexaenoic acid (22:6n3), which were reflected to different extents in the individual phospholipid classes. Thus, in addition to direct effects on cardiolipin composition and membrane remodeling, *Taz* deficiency elicits presumably compensatory effects on lipid metabolism that further alter mitochondrial membrane composition. Phospholipid

composition of SSM and IFM were nearly identical, indicating a similar effect of tafazzin on mitochondrial subpopulations.

Mitochondrial Respiratory Parameters

Oxidative phosphorylation (OXPHOS) rates were significantly lower in *Taz* vs. WT mitochondria when pyruvate + malate, palmitoylcarnitine + malate, or succinate + rotenone were used as substrates (Fig 4.2A). However, respiration rates were 69% and 46% higher in *Taz* compared to WT when glutamate + malate were used as substrates in SSM and IFM, respectively ($P < 0.01$), achieving levels that were comparable to those seen with pyruvate and palmitoylcarnitine in WT mitochondria. IFM respired at higher rates than SSM with all substrates in *Taz* and WT, but followed the same general trends in response to *Taz* deficiency. Mitochondrial yield from cardiac tissue was also higher in IFM and SSM, and tended to be slightly lower in *Taz* compared to WT animals (Fig 4.2B; $P = \text{NS}$). The enzymatic activity of ETS complex I and IV were 17% and 26% lower in *Taz* vs. WT IFM ($P < 0.05$; Fig 4.2C). Mitochondrial CoA content was 43% lower in *Taz* vs. WT ($P < 0.01$; Fig 4.2D).

Cardiac Metabolomic and Mitochondrial Proteomic Profiling

Cardiac metabolomic profiling revealed 16 metabolites with sufficient signal intensities for confident identification that were significantly different between *Taz* and WT (Table 4.1). The majority of these changes were 30-220% higher levels of amino acids in *Taz* vs. WT hearts, though not all amino acids were affected. Pantothenic acid, nicotinamide, taurine and proline were the only metabolites found to be significantly lower in *Taz* vs. WT.

Analysis of the *Taz* mitochondrial proteome identified 228 proteins of which were found to be significantly different between *Taz* and WT at $P < 0.1$ (Table 4.2). Twelve proteins were significantly higher in *Taz*, including stress response enzymes, acyl-CoA thioesterases, malate dehydrogenase, and cytochrome b_5 reductase. Nineteen proteins were found to be significantly lower in *Taz* vs. WT, including enzymes involved in amino acid catabolism, respiratory complex I assembly and fatty acid oxidation. An interpretive schematic integrating the majority of significant metabolomic and proteomic findings within the context of mitochondrial metabolism is presented in Figure 4.3.

Mitochondrial H₂O₂ release and oxidative stress

Taz mitochondrial H₂O₂ release was 28% and 47% lower in *Taz* compared to WT in SSM ($P = \text{NS}$) and IFM ($P = 0.05$) when succinate and rotenone were used as substrates, and not different when pyruvate + malate were used (Fig 4.4A). Maximal H₂O₂ release induced by the addition of antimycin A in the presence of succinate + rotenone tended to be lower in *Taz*, reaching statistical significance in IFM (Fig 4.4B). Mitochondrial levels of HNE-protein adducts were similar between *Taz* and WT (Fig 4.4C), suggesting minimal effects of *Taz* deficiency on mitochondrial oxidative stress.

Discussion

Cardiolipin is required for the optimal function of several enzymes and integral processes of the inner mitochondrial membrane. The highly conserved molecular symmetry of its tetra-acyl configuration suggests an important biological role, but specific influence of CL on mitochondrial physiology remains unclear. Loss of *Taz* function abolishes the compositional

uniformity of cardiolipin, leading to abnormalities in mitochondrial ultrastructure, respiratory chain defects and cardioskeletal myopathy in humans and/or experimental models [74, 80, 81, 91]. Herein, we provide the first detailed investigation of *Taz* deficiency in mammalian cardiac mitochondria. Our studies reveal unexpected substrate-specific effects on mitochondrial respiration and complex modulation of the mitochondrial proteome that provide novel insights into the biological function of cardiolipin remodeling.

Abundant biochemical evidence supports an essential role of cardiolipin in providing the structural and functional support to enzymes involved in oxidative phosphorylation (OXPHOS) [15, 92-94]. Specific impairments in the stability and enzymatic function of NADH-ubiquinone oxidoreductase (complex I) and cytochrome c oxidase (complex IV) have been reported in BTHS lymphoblasts and *Taz*-deficient yeast models [79, 93], suggesting that respiratory chain defects may be a central pathogenic feature of *Taz* deficiency. Consistent with this hypothesis, lower enzymatic activities of complexes I and IV were seen in *Taz* vs. WT mitochondria in the present study. Oxidative phosphorylation rates with succinate, which delivers reducing equivalents directly to ubiquinol in the respiratory chain via succinate dehydrogenase (complex II), was decreased by a similar magnitude, further supporting the existence of multiple respiratory chain defects.

However, a much more robust impairment of oxidative phosphorylation was seen when palmitoylcarnitine or pyruvate were used as substrates. Previous studies have suggested a dependence of pyruvate transport and carnitine-palmitoyltransferase enzymes on cardiolipin for their optimal function *in vitro* [95, 96], which could explain the marked decrease seen here in carbohydrate and fat oxidation. Alternatively, pyruvate and fatty acid oxidation in the presence of malate at saturating substrate concentrations depend exclusively on delivery of NADH to

complex I (complex I-linked respiration). Therefore, a greater relative impairment of complex I- vs. complex II-linked respiration may simply reflect a limitation of respiratory capacity by the observed defect in complex I activity. Destabilization of complex I and its interaction with other respiratory components (respiratory supercomplexes) have been reported in BTHS lymphoblasts [79]. Furthermore, recent studies have demonstrated the critical role of the protein acyl-CoA dehydrogenase family member 9 (ACAD9) in the assembly and/or activity of complex I [97, 98]. Congruent with these findings, our proteomic analysis revealed decreases in several complex I subunits in *Taz* mitochondria. A 3.6-fold increase in the stress-induced mitochondrial Lon-protease [99] suggests that the loss of complex I subunits might have resulted from proteolysis due to incomplete assembly of the complex. However, the respective roles and interaction of tafazzin, cardiolipin and ACAD9 in maintaining the structural integrity of complex I will require further investigation.

Complex IV is considered a rate-limiting step in oxidative phosphorylation; therefore the observed 26% reduction in its maximal activity might be expected to limit oxidative phosphorylation capacity with all respiratory substrates. However, glutamate + malate respiration, which was elevated in *Taz* compared to WT mitochondria, reached maximal phosphorylation rates that were comparable to those obtained with carbohydrate and fatty acid oxidation in WT per mg of mitochondrial protein. This indicates that enzymatic capacity of complexes I and IV assayed in mitochondrial lysates, while defective, do not significantly limit oxidative phosphorylation capacity in *Taz* mitochondria. A compensatory upregulation of glutamate oxidation in *Taz* deficient mitochondria is consistent with evidence of enhanced proteolysis and reliance on gluconeogenesis in BTHS patients [100]. Cardiac metabolomics in the present study revealed an accumulation of several anaplerotic amino acids in *Taz* shRNA mice, which further

reflects a proteolytic phenotype. However, not all amino acids were elevated in *Taz* vs. WT hearts, suggesting a more specific phenomenon might be involved.

Perhaps the most striking finding in our metabolomic screening was a highly significant 41% decrease in pantothenic acid, an essential precursor for coenzyme-A (CoA) biosynthesis. Subsequent assay of CoA levels in *Taz* mitochondria revealed a similar 43% decrease compared to WT mitochondria. Oxidation of pyruvate, fatty acids, and several amino acid substrates requires entry into the TCA cycle as acetyl-CoA, which combines with oxaloacetate to form citrate in the citrate synthase reaction (Fig 4.3). Conversely, oxidation of glutamate in the presence of malate bypasses both acetyl-CoA formation and citrate synthase for direct oxidation by glutamate dehydrogenase or drives malate oxidation by malate dehydrogenase (MDH) via the malate-aspartate shuttle. In the presence of saturating substrate concentrations in cardiac mitochondria, the latter pathway predominates, leading to an inhibition of TCA flux upstream of MDH, promoting the exchange of 2-oxo-glutarate for malate, and removal of oxaloacetate as aspartate. Thus, in isolated mitochondria, glutamate + malate respiration is essentially supported by NADH generation by MDH [101], which was elevated in *Taz* vs. WT mitochondria. The significance of this finding is that, in contrast to pyruvate and fatty acid supported respiration, glutamate + malate respiration is independent of CoA. Taken together, these data suggest that impairment of CoA biosynthesis, transport and/or utilization may underlie the substrate-specific impairment of respiratory function in *Taz*-deficient mitochondria. The mechanisms by which tafazzin specifically influence these processes remains unclear and warrants further investigation.

An alternative hypothesis is that *Taz* deficiency selectively reduces mitochondrial content of enzymes involved in metabolic pathways that utilize CoA as a cofactor. In *Saccharomyces*

cerevisiae, cardiolipin has been shown to play a key role in mitochondrial protein import [78, 102]. While several proteins were decreased in *Taz* versus WT in our proteomic analysis, many others remained unchanged or elevated, arguing against a global impairment of mitochondrial protein import. Additionally, two mitochondrial encoded-proteins, NU2M and NU1M were decreased in *Taz* compared to WT. No overt distinguishing characteristics of nuclear encoded proteins (e.g., hydrophobicity score) were evident among those lower in *Taz* vs. WT mitochondria.

In addition to metabolic derangements, dysfunctional mitochondria may contribute to pathology by releasing excessive amounts of reactive oxygen species (ROS) that can damage cellular lipids, proteins and DNA. Unexpectedly, despite defects in respiratory complexes I and IV, mitochondrial H₂O₂ release was similar between *Taz* and WT when provided pyruvate + malate as a substrate, and lower in *Taz* when provided succinate + rotenone. Maximal H₂O₂ release with succinate + rotenone in the presence of antimycin A remained lower in *Taz* compared to WT, indicating a reduced capacity to generate ROS from complex III. There were no measurable differences in 4-HNE-protein adducts content between *Taz* and WT, further suggesting that oxidative stress is unlikely to be a pathogenic feature of *Taz* deficiency. However, it is worth noting that although total 4-HNE-protein adducts appear unaltered, there appears to be an unexplainable higher molecular weight band that is elevated in *Taz*. This warrants further inquiry into additional measurements of markers for oxidative stress.

In Barth syndrome, the absence of functional tafazzin results in compromised cristae formation. A recent seminal paper by Schlame et al., demonstrated tafazzin to be a non-specific phospholipid transacylase that reacts with cardiolipin in specialized monolayer membrane domains of high curvature, such as those found in mitochondrial cristae [64]. The selective LA

enrichment of cardiolipin in mammalian heart mitochondria appears to result from the “packing” properties and bioavailability of this fatty acid rather than an acyl specificity of the tafazzin enzyme itself [64, 103]. Collectively, these findings suggest the cardiolipin remodeling process itself and/or tafazzin enzyme may play a more important and specific role than the resulting composition of cardiolipin in supporting cardiac mitochondrial function.

In summary, our studies indicate that *Taz* deficiency selectively impairs carbohydrate and fatty acid oxidation in cardiac mitochondria and elicits a compensatory increase in glutamate oxidation capacity that supports normal rates of oxidative phosphorylation despite defects in respiratory chain enzyme function. Cardiac metabolomic and mitochondrial proteomic screenings revealed a complex array of changes consistent with impaired assembly of mitochondrial proteins and reduced synthesis and/or utilization of CoA, which may compound or reflect direct effects of altered cardiolipin metabolism on mitochondrial membrane function. Despite these perturbations, *Taz* deficiency appears not to increase mitochondrial ROS release or lipid peroxidation. In conclusion, our studies suggest that impairment of intermediary metabolic substrate utilization is the central bioenergetic consequence of *Taz* deficiency and propose that perhaps it is the impairment of the tafazzin-mediated CL remodeling process itself, not the resulting change in cardiolipin composition, which causes the mitochondrial respiratory dysfunction in Barth syndrome.

Table 4.1. Cardiac metabolome screening results

Identified Metabolite	WT	<i>Taz</i> shRNA	%WT	P-value
<u>Greater in <i>Taz</i> shRNA</u>				
Threonine (Thr)	585 ± 68	768 ± 103	131	0.019
Alanine (Ala)	8804 ± 1666	12054 ± 578	137	0.004
Phenylalanine (Phe)	197 ± 22	287 ± 22	145	0.002
Serine (Ser)	1189 ± 220	1837 ± 209	154	0.003
Leucine (Leu)	717 ± 110	1245 ± 248	174	0.006
Valine (Val)	515 ± 63	946 ± 141	184	>0.001
Glycerolipid	68 ± 9	142 ± 24	210	>0.001
Tyrosine (Tyr)	205 ± 85	440 ± 84	214	0.004
Lysine (Lys)	294 ± 89	689 ± 202	235	0.009
Aspartate (Asp)	2970 ± 1470	7346 ± 686	247	>0.001
Inosine (Ino)	49 ± 21	151 ± 30	309	0.014
Glycine (Gly)	2584 ± 194	8266 ± 579	320	>0.001
<u>Lower in <i>Taz</i> in shRNA</u>				
Pantothenic Acid	150 ± 14	89 ± 4	59	>0.001
Nicotinamide	867 ± 91	693 ± 32	79	0.004
Taurine	26371 ± 1925	21524 ± 701	82	0.001
Proline (Pro)	30559 ± 2677	25601 ± 2291	131	0.019

Metabolites listed are all those found to be significantly different between *Taz* and WT hearts at $P < 0.05$ with sufficient signal intensities for confident identification. Relative metabolite quantities are provided for WT and *Taz* as mean ± SEM area of the GC peak. %WT = Level of metabolite present in *Taz* hearts expressed as a percent of the mean WT value for each metabolite.

Table 4.2. Mitochondrial proteomic profiling results

Identified Protein	Accession Number	Swiss Access#	<i>Taz</i>/WT	P-value	HFPBY Score
<u>Higher in <i>Taz</i> shRNA</u>					
NADH-cytochrome b5 reductase	NB5R1	Q9DB73	9.96	0.00021	-0.138
Lon protease homolog	E9Q120	Q8CGK3	3.53	0.00051	-0.315
Heat shock protein 75 kDa	F6YP65	Q9CQN1	2.85	0.015	-0.357
Stress-70 protein	GRP75	P38647	2.04	0.03	-0.394
Methylcrotonoyl-CoA carboxylase subunit alpha	MCCA	Q99MR8	1.99	0.0037	-0.305
Acyl-coenzyme A thioesterase 13	ACO13	Q9CQR4	1.90	0.021	0.009
Acyl-coenzyme A thioesterase 2	ACOT2	Q9QYR9	1.88	0.0066	-0.123
Dihydrolipoyllysine-residue acetyltransferase	ODP2	Q8BMF4	1.43	0.0088	0.029
Malate dehydrogenase	MDHM	P08249	1.40	0.018	0.136
Platelet glycoprotein 4	CD36	Q08857	1.36	0.0025	-0.053
<u>Lower in <i>Taz</i> in shRNA</u>					
Methylcrotonoyl-Coenzyme A carboxylase 2 (Beta)	B2RUK5	Q3ULD5	0.19	0.021	-0.165
Acyl-CoA dehydrogenase family member 9	ACAD9	Q8JZN5	0.25	0.016	-0.058
Mitochondrial pyruvate carrier 2	MPC2	Q9D023	0.31	0.064	0.124
Long-chain-fatty-acid--CoA ligase 1	ACSL1	P41216	0.32	0.026	-0.045
Amine oxidase	AOFB	Q8BW75	0.35	0.031	-0.195
NADH-ubiquinone oxidoreductase chain 2	NU2M	P03893	0.35	0.066	0.799
NADH dehydrogenase 1 alpha subcomplex subunit 12	NDUAC	Q7TMF3	0.39	0.085	-0.777

NADH dehydrogenase ubiquinone 1 alpha subcomplex subunit 8	NDUAB	Q9DCJ5	0.60	0.056	-0.626
Protein Ogdhl	E9Q7L0	E9Q7L0	0.62	0.036	-0.296
NADH-ubiquinone oxidoreductase chain 1	NU1M	P03888	0.64	0.065	0.737
Peroxiredoxin-5	H3BJQ7	P99029	0.68	0.044	0.175
NADH dehydrogenase alpha subcomplex subunit 10	NDUAA	Q99LC3	0.68	0.021	-0.505
Medium-chain specific acyl-CoA dehydrogenase	ACADM	P45952	0.68	0.058	-0.291
NADH dehydrogenase iron-sulfur protein 5	NDUS5	Q99LY9	0.69	0.052	-1.029
NADH dehydrogenase 1 alpha subcomplex subunit 9	NDUA9	Q9DC69	0.72	0.071	-0.121
2,4-dienoyl-CoA reductase	DECR	Q9CQ62	0.74	0.064	-0.078
Mitochondrial 2-oxoglutarate/malate carrier protein	M2OM	Q9CR62	0.80	0.061	0.072
Cytochrome b-c1 complex subunit 7	Q9CQB4	Q9D855	0.80	0.069	-1.066
Succinyl-CoA ligase	SUCB1	Q9Z2I9	0.82	0.032	0.032

Proteins listed are those found to be significantly different by spectral counting between *Taz* and WT hearts at $P < 0.085$ meeting the validation criteria described in the Methods. Relative quantities of proteins determined by spectral counting are presented as *Taz*/WT, with respective P-values from independent sample t-tests. HFPBY= protein hydrophobicity score derived from ExPASy (<http://www.expasy.org>), the DIB Bioinformatic Resource Portal. The GRAVY value for a protein is calculated as the sum of hydropathy values of all the amino acids, divided by the number of residues in the sequence as determined by Kyte and Doolittle.

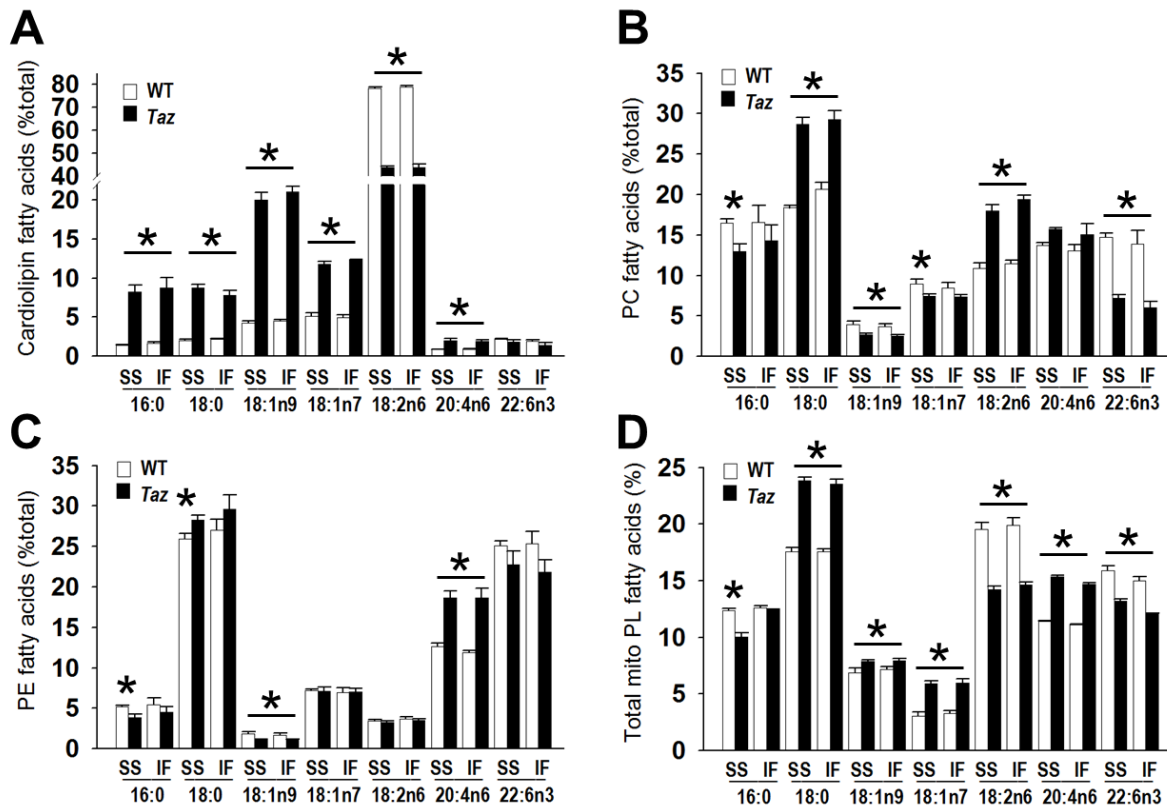


Figure 4.1. Mitochondrial phospholipid composition

Gas chromatographic analyses of major fatty acids present in cardioliplin (A), phosphatidylcholine (B), phosphatidylethanolamine (C) and total phospholipids (D) in subarcolemmal (SS) and intermyofibrillar (IF) mitochondria isolated from *Taz* shRNA (n = 8) and WT hearts (n = 6). Fatty acid abbreviations are as follows: 16:0, palmitate; 18:0, stearate; 18:1n9, oleate; 18:7n7, vaccinate; 18:2n6, linoleate; 20:4n6, arachidonate; and 22:6n3, docosahexanoate. All data are means \pm SEM. *P < 0.05 *Taz* vs. WT.

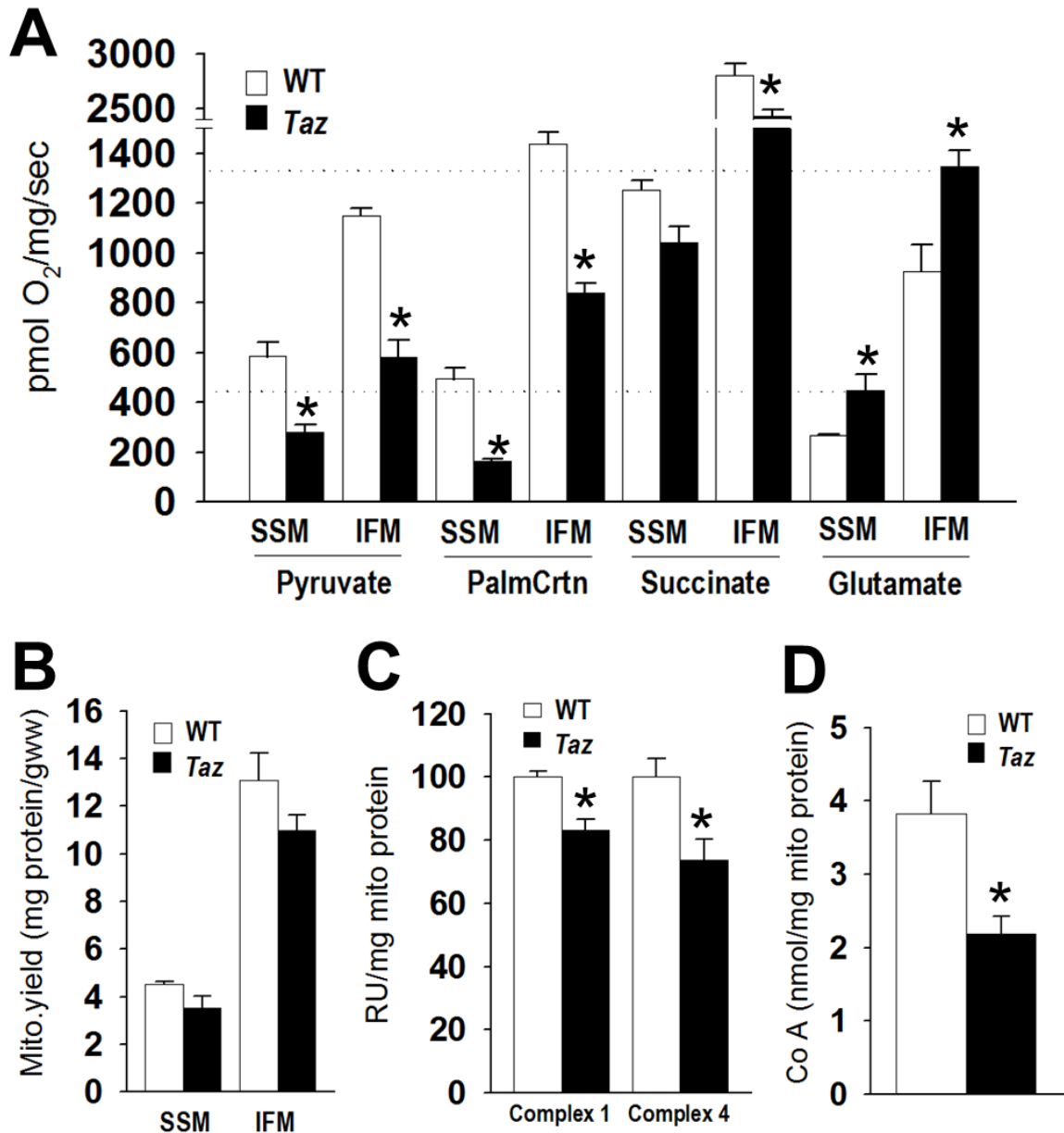


Figure 4.2. Mitochondria respiratory parameters

A) Oxidative phosphorylation rates using pyruvate + malate (Pyruvate), palmitoylcarnitine + malate (PalmCrtn), succinate + rotenone (Succinate), and glutamate + malate (Glutamate) as substrates in subsarcolemmal (SSM) and intermyofibrillar (IFM) mitochondria (n = 8-12/group). B) Protein yield of mitochondrial isolation per gram of cardiac tissue (n = 8/group). C) Enzymatic activities of respiratory chain complexes 1 and IV and D) coenzyme A levels in isolated IF mitochondria (n = 8/ group). All data are means ± SEM. *P < 0.05 vs. WT.

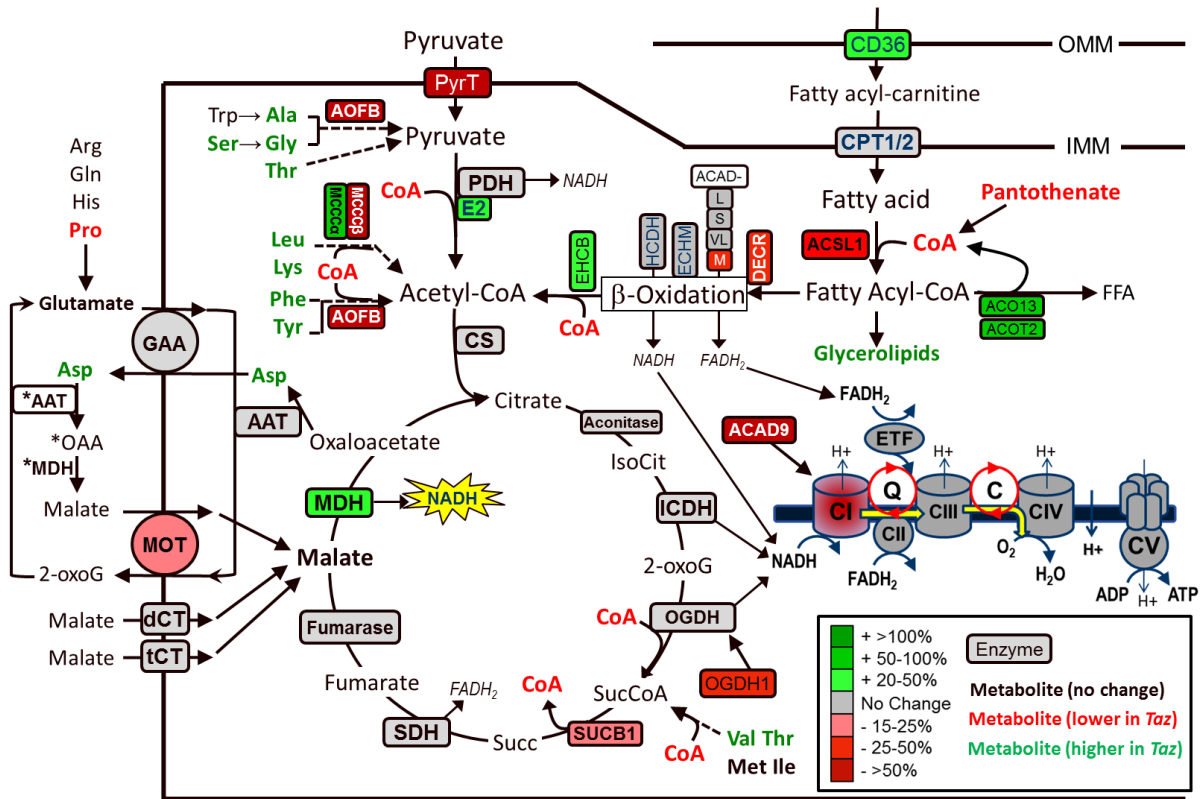


Figure 4.3. Integrative summary of significant findings from metabolomic and proteomic profiling

See Tables 1 and 2 and below for abbreviations and the inset legend for symbols and color-coding. Briefly, enzymes and metabolites in red were lower in *Taz* vs. WT, while green indicates higher levels in *Taz* vs. WT. Dotted lines indicate multiple reactions not shown. Several intermediary steps and pathway interactions have been omitted or simplified for clarity. Abbreviations (not included in text or Tables 1 and 2): dCT, dicarboxylate transporter; tCT, tricarboxylate transporter; GAA, glutamate-aspartate antiporter; MOT, malate-oxaloacetate translocase. *Cytosolic AAT and MDH are not present in mitochondrial proteomic or respirometry studies, but are included for integral interpretation.

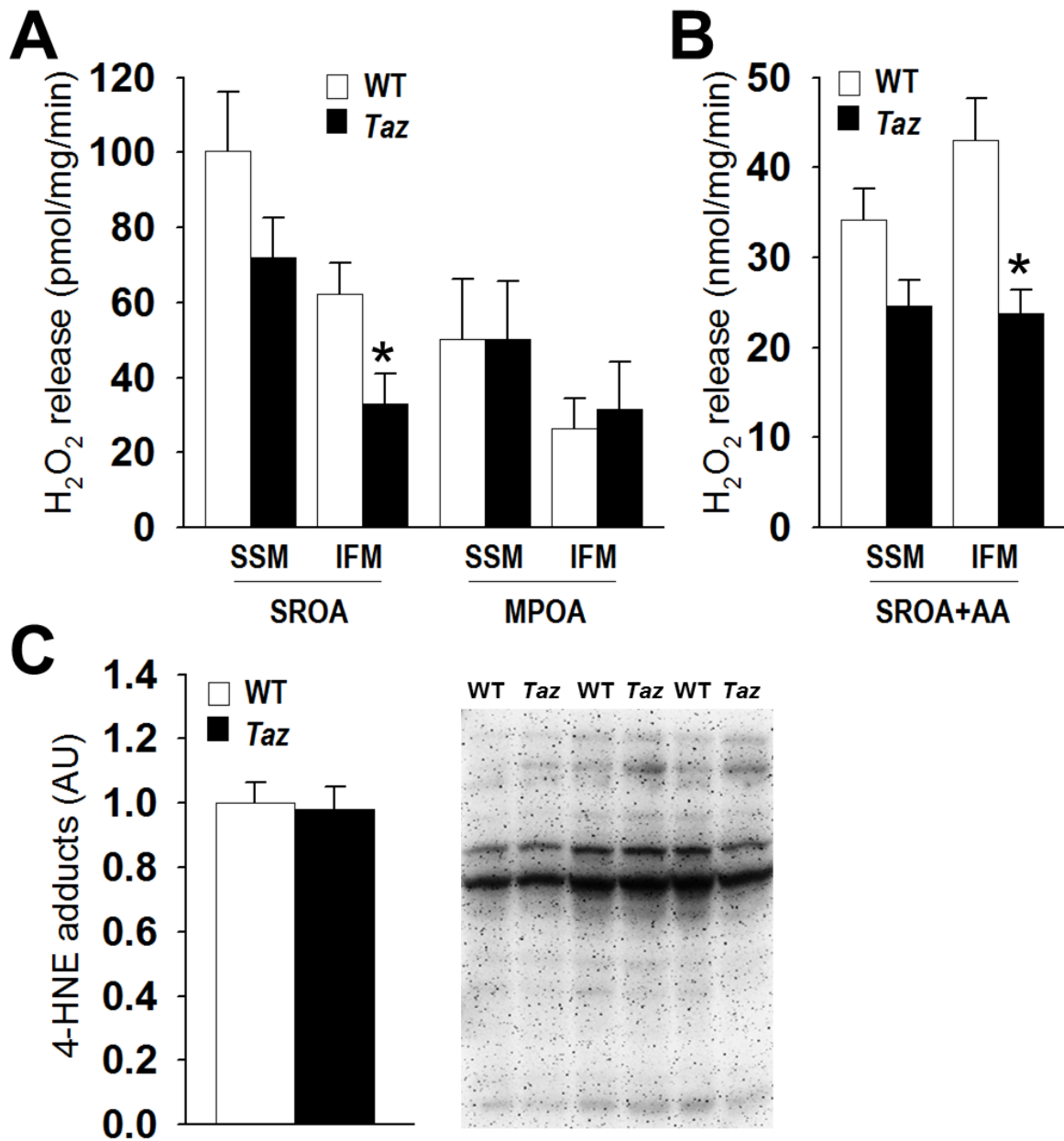


Figure 4.4. Mitochondrial oxidative stress

A) Mitochondrial H_2O_2 release using succinate + rotenone (SROA; $n = 8$) and malate + pyruvate (MPOA; $n = 8$) as substrates in subsarcolemmal (SSM) and intermyofibrillar mitochondria (IFM). B) Maximal rates of mitochondrial H_2O_2 release using succinate + rotenone in the presence of antimycin A (SROA+AA; $n = 6$). C) Densitometry and representative blotting of mitochondrial 4-HNE-protein adducts from *Taz* and WT IF mitochondria ($n = 8$). All data are means \pm SEM. * $P < 0.05$.

CHAPTER V – OVERALL CONCLUSIONS

This collection of work presents novel and significant insight into the physiological implications of cardiolipin remodeling observed in cardiac pathologies. First, we show that cardiolipin remodeling observed in the aged and failing heart is due at least in part to increased polyunsaturated fatty acid metabolism through the delta-6 desaturase pathway, leading to the signature loss of linoleic acid and corresponding increases in long-chain PUFAs observed in several pathologies. This process appears to be critical in the pathogenesis of maladaptive remodeling by mechanisms currently being investigated in our lab. However, contrary to our hypothesis, studies in Chapters II and III indicated that despite close correlation, there appears to be no independent effect of altered cardiolipin composition on cardiac mitochondrial respiratory function in aging and heart failure. Second, we provide the first characterization of mitochondrial respiratory function in tafazzin-deficient heart, demonstrating that *Taz* deficiency selectively impairs carbohydrate and fatty acid oxidation in cardiac mitochondria. Unexpectedly, we also found evidence for impaired assembly of mitochondrial proteins and strikingly, reduced synthesis and/or utilization of CoA, which may reflect direct or compensatory effects of altered cardiolipin metabolism on mitochondria. This suggests that perhaps it is impairment of the tafazzin-mediated *CL remodeling process* itself, not the resulting change in cardiolipin composition, which causes the mitochondrial respiratory dysfunction in Barth syndrome.

Taken together, these studies challenge previous reports that have suggested alterations of the distinctly uniform and symmetric fatty acyl chain composition of cardiolipin impair cardiac mitochondrial respiration. Rather, these findings instead show that the widely observed redistribution of cardiolipin PUFA content in chronic cardiac pathologies appears to reflect a global increase in PUFA metabolism via the D6D pathway, which profoundly influences cardiac

structure and function by mechanisms we are only beginning to comprehend. Interestingly, defects in the cardiolipin remodeling process itself and/or tafazzin enzyme may play a distinct and perhaps more important role in cardiac mitochondrial respiratory function and cardiomyopathy than previously thought.

Future Directions

To further elucidate the influence of D6D on cardiac health, we recently generated a novel transgenic mouse line with global overexpression of the D6D gene (*Fads2*). These mice are currently in their 4th backcross generation and exhibit expected changes in myocardial membrane phospholipid composition (lower LA and higher AA and DHA), increased eicosanoid levels in heart and liver, and mild cardiac hypertrophy and contractile dysfunction compared to wild-type littermates. We plan to stress the model with exercise, aortic banding and perhaps other stimuli to establish the role of D6D in responses to physiologic and pathologic stress, followed by mechanistic studies evaluating the contribution of effects on inflammatory, metabolic, and hypertrophy signaling pathways.

Recently, we received a second grant from the Barth Syndrome Foundation to further investigate the mechanisms responsible for our observation of substrate-specific impairment of mitochondrial respiration in the *Taz*-shRNA mice. Specific aims include an examination of the influence fatty acid transport exerts on the observed impairment of fatty acid oxidation, and a series of studies investigating the potential effects of *Taz* deficiency on the intestinal absorption of pantothenic acid and utilization/transport of CoA in cardiac mitochondria using mice from our *Taz*-shRNA colony.

REFERENCES

1. Dai, D.F., et al., *Cardiac aging: from molecular mechanisms to significance in human health and disease*. *Antioxid Redox Signal*, 2012. **16**(12): p. 1492-526.
2. Lakatta, E.G. and D. Levy, *Arterial and cardiac aging: major shareholders in cardiovascular disease enterprises: Part II: the aging heart in health: links to heart disease*. *Circulation*, 2003. **107**(2): p. 346-54.
3. Chaudhary, K.R., H. El-Sikhry, and J.M. Seubert, *Mitochondria and the aging heart*. *J Geriatr Cardiol*, 2011. **8**(3): p. 159-67.
4. Dai, D.F. and P.S. Rabinovitch, *Cardiac aging in mice and humans: the role of mitochondrial oxidative stress*. *Trends Cardiovasc Med*, 2009. **19**(7): p. 213-20.
5. Fannin, S.W., et al., *Aging selectively decreases oxidative capacity in rat heart inter-fibrillar mitochondria*. *Arch Biochem Biophys*, 1999. **372**(2): p. 399-407.
6. Tamburini, I., et al., *Effects of dietary restriction on age-related changes in the phospholipid fatty acid composition of various rat tissues*. *Aging Clin Exp Res*, 2004. **16**(6): p. 425-31.
7. Gudbjarnason, S., *Pathophysiology of long-chain polyene fatty acids in heart muscle*. *Nutr Metab*, 1980. **24 Suppl 1**: p. 142-6.
8. Lee, H.J., et al., *Selective remodeling of cardiolipin fatty acids in the aged rat heart*. *Lipids Health Dis*, 2006. **5**: p. 2.
9. Quiles, J.L., et al., *Ageing-related tissue-specific alterations in mitochondrial composition and function are modulated by dietary fat type in the rat*. *J Bioenerg Biomembr*, 2002. **34**(6): p. 517-24.
10. Pamplona, R., et al., *Double bond content of phospholipids and lipid peroxidation negatively correlate with maximum longevity in the heart of mammals*. *Mech Ageing Dev*, 2000. **112**(3): p. 169-83.
11. Pamplona, R., G. Barja, and M. Portero-Otin, *Membrane fatty acid unsaturation, protection against oxidative stress, and maximum life span: a homeoviscous-longevity adaptation?* *Ann N Y Acad Sci*, 2002. **959**: p. 475-90.

12. Pepe, S., *Effect of dietary polyunsaturated fatty acids on age-related changes in cardiac mitochondrial membranes*. *Exp Gerontol*, 2005. **40**(8-9): p. 751-8.
13. Pamplona, R., et al., *Mitochondrial membrane peroxidizability index is inversely related to maximum life span in mammals*. *J Lipid Res*, 1998. **39**(10): p. 1989-94.
14. Lewin, M.B. and P.S. Timiras, *Lipid changes with aging in cardiac mitochondrial membranes*. *Mech Ageing Dev*, 1984. **24**(3): p. 343-51.
15. Chicco, A.J. and G.C. Sparagna, *Role of cardiolipin alterations in mitochondrial dysfunction and disease*. *Am J Physiol Cell Physiol*, 2007. **292**(1): p. C33-44.
16. Sparagna, G.C., et al., *Loss of cardiac tetralinoleoyl cardiolipin in human and experimental heart failure*. *J Lipid Res*, 2007. **48**(7): p. 1559-70.
17. Obukowicz, M.G., et al., *Novel, selective delta6 or delta5 fatty acid desaturase inhibitors as antiinflammatory agents in mice*. *J Pharmacol Exp Ther*, 1998. **287**(1): p. 157-66.
18. Pamplona, R., et al., *Low fatty acid unsaturation: a mechanism for lowered lipoperoxidative modification of tissue proteins in mammalian species with long life spans*. *J Gerontol A Biol Sci Med Sci*, 2000. **55**(6): p. B286-91.
19. Chen, Q. and E.J. Lesnefsky, *Depletion of cardiolipin and cytochrome c during ischemia increases hydrogen peroxide production from the electron transport chain*. *Free Radic Biol Med*, 2006. **40**(6): p. 976-82.
20. Warensjo, E., et al., *Markers of dietary fat quality and fatty acid desaturation as predictors of total and cardiovascular mortality: a population-based prospective study*. *Am J Clin Nutr*, 2008. **88**(1): p. 203-9.
21. Claypool, S.M. and C.M. Koehler, *The complexity of cardiolipin in health and disease*. *Trends Biochem Sci*, 2012. **37**(1): p. 32-41.
22. Picard, M., et al., *Mitochondrial function in permeabilized cardiomyocytes is largely preserved in the senescent rat myocardium*. *PLoS One*, 2012. **7**(8): p. e43003.

23. Choksi, K.B. and J. Papaconstantinou, *Age-related alterations in oxidatively damaged proteins of mouse heart mitochondrial electron transport chain complexes*. Free Radic Biol Med, 2008. **44**(10): p. 1795-805.
24. Kumaran, S., et al., *Age-associated decreased activities of mitochondrial electron transport chain complexes in heart and skeletal muscle: role of L-carnitine*. Chem Biol Interact, 2004. **148**(1-2): p. 11-8.
25. Hong, M.Y., et al., *Fish oil increases mitochondrial phospholipid unsaturation, upregulating reactive oxygen species and apoptosis in rat colonocytes*. Carcinogenesis, 2002. **23**(11): p. 1919-25.
26. Li, J., et al., *Cardiolipin remodeling by ALCAT1 links oxidative stress and mitochondrial dysfunction to obesity*. Cell Metab, 2010. **12**(2): p. 154-65.
27. Saito, M. and K. Kubo, *Relationship between tissue lipid peroxidation and peroxidizability index after alpha-linolenic, eicosapentaenoic, or docosahexaenoic acid intake in rats*. Br J Nutr, 2003. **89**(1): p. 19-28.
28. Saito, M., *Dietary docosahexaenoic acid does not promote tissue lipid peroxide formation to the extent expected from the peroxidizability index of the lipids*. Biofactors, 2000. **13**(1-4): p. 15-24.
29. Terzioglu, M. and N.G. Larsson, *Mitochondrial dysfunction in mammalian ageing*. Novartis Found Symp, 2007. **287**: p. 197-208; discussion 208-13.
30. Lesnefsky, E.J. and C.L. Hoppel, *Ischemia-reperfusion injury in the aged heart: role of mitochondria*. Arch Biochem Biophys, 2003. **420**(2): p. 287-97.
31. Leslie, C.C., *Regulation of arachidonic acid availability for eicosanoid production*. Biochem Cell Biol, 2004. **82**(1): p. 1-17.
32. Jenkins, C.M., A. Cedars, and R.W. Gross, *Eicosanoid signalling pathways in the heart*. Cardiovasc Res, 2009. **82**(2): p. 240-9.
33. Zhang, Z., et al., *COX-2-dependent cardiac failure in Gh/tTG transgenic mice*. Circ Res, 2003. **92**(10): p. 1153-61.

34. Kayama, Y., et al., *Cardiac 12/15 lipoxygenase-induced inflammation is involved in heart failure*. J Exp Med, 2009. **206**(7): p. 1565-74.
35. Graham, D.A. and J.W. Rush, *Cyclooxygenase and thromboxane/prostaglandin receptor contribute to aortic endothelium-dependent dysfunction in aging female spontaneously hypertensive rats*. J Appl Physiol, 2009. **107**(4): p. 1059-67.
36. Kunapuli, P., et al., *Prostaglandin F2alpha (PGF2alpha) and the isoprostane, 8, 12-iso-isoprostane F2alpha-III, induce cardiomyocyte hypertrophy. Differential activation of downstream signaling pathways*. J Biol Chem, 1998. **273**(35): p. 22442-52.
37. Levy, D., et al., *The progression from hypertension to congestive heart failure*. JAMA, 1996. **275**(20): p. 1557-62.
38. Yndestad, A., et al., *Role of inflammation in the progression of heart failure*. Curr Cardiol Rep, 2007. **9**(3): p. 236-41.
39. Dhalla, A.K., M.F. Hill, and P.K. Singal, *Role of oxidative stress in transition of hypertrophy to heart failure*. J Am Coll Cardiol, 1996. **28**(2): p. 506-14.
40. Neubauer, S., *The failing heart--an engine out of fuel*. N Engl J Med, 2007. **356**(11): p. 1140-51.
41. Kang, P.M. and S. Izumo, *Apoptosis and heart failure: A critical review of the literature*. Circ Res, 2000. **86**(11): p. 1107-13.
42. Heerdt, P.M., et al., *Disease-specific remodeling of cardiac mitochondria after a left ventricular assist device*. Ann Thorac Surg, 2002. **73**(4): p. 1216-21.
43. Reibel, D.K., et al., *Altered phospholipid metabolism in pressure-overload hypertrophied hearts*. Am J Physiol, 1986. **250**(1 Pt 2): p. H1-6.
44. Sparagna, G.C., et al., *Quantitation of cardiolipin molecular species in spontaneously hypertensive heart failure rats using electrospray ionization mass spectrometry*. J Lipid Res, 2005. **46**(6): p. 1196-204.
45. Nasa, Y., et al., *Changes in fatty acid compositions of myocardial lipids in rats with heart failure following myocardial infarction*. Mol Cell Biochem, 1997. **176**(1-2): p. 179-89.

46. Han, X., et al., *Alterations in myocardial cardiolipin content and composition occur at the very earliest stages of diabetes: a shotgun lipidomics study*. *Biochemistry*, 2007. **46**(21): p. 6417-28.
47. Nakamura, M.T. and T.Y. Nara, *Structure, function, and dietary regulation of delta6, delta5, and delta9 desaturases*. *Annu Rev Nutr*, 2004. **24**: p. 345-76.
48. Heyen, J.R., et al., *Structural, functional, and molecular characterization of the SHHF model of heart failure*. *Am J Physiol Heart Circ Physiol*, 2002. **283**(5): p. H1775-84.
49. Mulligan, C.M., et al., *Dietary linoleate preserves cardiolipin and attenuates mitochondrial dysfunction in the failing rat heart*. *Cardiovasc Res*, 2012. **94**(3): p. 460-8.
50. Zarini, S., et al., *Transcellular biosynthesis of cysteinyl leukotrienes in vivo during mouse peritoneal inflammation*. *Proc Natl Acad Sci U S A*, 2009. **106**(20): p. 8296-301.
51. Switzer, B.R. and G.K. Summer, *Improved method for hydroxyproline analysis in tissue hydrolyzates*. *Anal Biochem*, 1971. **39**(2): p. 487-91.
52. Keith, M., et al., *Increased oxidative stress in patients with congestive heart failure*. *J Am Coll Cardiol*, 1998. **31**(6): p. 1352-6.
53. Claypool, S.M. and C.M. Koehler, *The complexity of cardiolipin in health and disease*. *Trends Biochem Sci*. **37**(1): p. 32-41.
54. Murray, A.J., et al., *Increased mitochondrial uncoupling proteins, respiratory uncoupling and decreased efficiency in the chronically infarcted rat heart*. *J Mol Cell Cardiol*, 2008. **44**(4): p. 694-700.
55. McHowat, J., et al., *Redistribution and abnormal activity of phospholipase A(2) isoenzymes in postinfarct congestive heart failure*. *Am J Physiol Cell Physiol*, 2001. **280**(3): p. C573-80.
56. Wen, Y., et al., *Overexpression of 12-lipoxygenase and cardiac fibroblast hypertrophy*. *Trends Cardiovasc Med*, 2003. **13**(4): p. 129-36.
57. Gordon, J.W., J.A. Shaw, and L.A. Kirshenbaum, *Multiple facets of NF-kappaB in the heart: to be or not to NF-kappaB*. *Circ Res*. **108**(9): p. 1122-32.

58. Vanderheyden, M., et al., *Myocardial cytokine gene expression is higher in aortic stenosis than in idiopathic dilated cardiomyopathy*. Heart, 2005. **91**(7): p. 926-31.
59. Hamid, T., et al., *Cardiomyocyte NF-kappaB p65 promotes adverse remodelling, apoptosis, and endoplasmic reticulum stress in heart failure*. Cardiovasc Res. **89**(1): p. 129-38.
60. Barth, P.G., et al., *An X-linked mitochondrial disease affecting cardiac muscle, skeletal muscle and neutrophil leucocytes*. J Neurol Sci, 1983. **62**(1-3): p. 327-55.
61. Barth, P.G., et al., *X-linked cardioskeletal myopathy and neutropenia (Barth syndrome): an update*. Am J Med Genet A, 2004. **126A**(4): p. 349-54.
62. Bione, S., et al., *A novel X-linked gene, G4.5. is responsible for Barth syndrome*. Nat Genet, 1996. **12**(4): p. 385-9.
63. Bolhuis, P.A., et al., *Mapping of the locus for X-linked cardioskeletal myopathy with neutropenia and abnormal mitochondria (Barth syndrome) to Xq28*. Am J Hum Genet, 1991. **48**(3): p. 481-5.
64. Schlame, M., et al., *The physical state of lipid substrates provides transacylation specificity for tafazzin*. Nat Chem Biol, 2012.
65. Hoch, F.L., *Cardiolipins and biomembrane function*. Biochim Biophys Acta, 1992. **1113**(1): p. 71-133.
66. Fry, M. and D.E. Green, *Cardiolipin requirement by cytochrome oxidase and the catalytic role of phospholipid*. Biochem Biophys Res Commun, 1980. **93**(4): p. 1238-46.
67. Fry, M. and D.E. Green, *Cardiolipin requirement for electron transfer in complex I and III of the mitochondrial respiratory chain*. J Biol Chem, 1981. **256**(4): p. 1874-80.
68. Robinson, N.C., *Functional binding of cardiolipin to cytochrome c oxidase*. J Bioenerg Biomembr, 1993. **25**(2): p. 153-63.
69. Schlame, M., D. Rua, and M.L. Greenberg, *The biosynthesis and functional role of cardiolipin*. Prog Lipid Res, 2000. **39**(3): p. 257-88.

70. Sparagna, G.C. and E.J. Lesnefsky, *Cardiolipin remodeling in the heart*. J Cardiovasc Pharmacol, 2009. **53**(4): p. 290-301.
71. Xu, Y., et al., *The enzymatic function of tafazzin*. J Biol Chem, 2006. **281**(51): p. 39217-24.
72. Schlame, M., et al., *Phospholipid abnormalities in children with Barth syndrome*. J Am Coll Cardiol, 2003. **42**(11): p. 1994-9.
73. Valianpour, F., et al., *Monolysocardiolipins accumulate in Barth syndrome but do not lead to enhanced apoptosis*. J Lipid Res, 2005. **46**(6): p. 1182-95.
74. Xu, Y., et al., *Characterization of lymphoblast mitochondria from patients with Barth syndrome*. Lab Invest, 2005. **85**(6): p. 823-30.
75. Khuchua, Z., et al., *A zebrafish model of human Barth syndrome reveals the essential role of tafazzin in cardiac development and function*. Circ Res, 2006. **99**(2): p. 201-8.
76. Xu, Y., et al., *A Drosophila model of Barth syndrome*. Proc Natl Acad Sci U S A, 2006. **103**(31): p. 11584-8.
77. Chen, S., Q. He, and M.L. Greenberg, *Loss of tafazzin in yeast leads to increased oxidative stress during respiratory growth*. Mol Microbiol, 2008. **68**(4): p. 1061-72.
78. Joshi, A.S., et al., *Cellular functions of cardiolipin in yeast*. Biochim Biophys Acta, 2009. **1793**(1): p. 212-8.
79. McKenzie, M., et al., *Mitochondrial respiratory chain supercomplexes are destabilized in Barth Syndrome patients*. J Mol Biol, 2006. **361**(3): p. 462-9.
80. Soustek, M.S., et al., *Characterization of a transgenic short hairpin RNA-induced murine model of Tafazzin deficiency*. Hum Gene Ther. **22**(7): p. 865-71.
81. Acehan, D., et al., *Cardiac and skeletal muscle defects in a mouse model of human Barth syndrome*. J Biol Chem. **286**(2): p. 899-908.

82. Palmer, J.W., B. Tandler, and C.L. Hoppel, *Biochemical properties of subsarcolemmal and interfibrillar mitochondria isolated from rat cardiac muscle*. J Biol Chem, 1977. **252**(23): p. 8731-9.
83. Soustek, M.S., et al., *Characterization of a transgenic short hairpin RNA-induced murine model of Tafazzin deficiency*. Hum Gene Ther, 2011. **22**(7): p. 865-71.
84. Acehan, D., et al., *Cardiac and skeletal muscle defects in a mouse model of human Barth syndrome*. J Biol Chem, 2011. **286**(2): p. 899-908.
85. Kall, L., et al., *Assigning significance to peptides identified by tandem mass spectrometry using decoy databases*. J Proteome Res, 2008. **7**(1): p. 29-34.
86. Keller, A., et al., *Empirical statistical model to estimate the accuracy of peptide identifications made by MS/MS and database search*. Anal Chem, 2002. **74**(20): p. 5383-92.
87. Searle, B.C., M. Turner, and A.I. Nesvizhskii, *Improving sensitivity by probabilistically combining results from multiple MS/MS search methodologies*. J Proteome Res, 2008. **7**(1): p. 245-53.
88. Liu, H., R.G. Sadygov, and J.R. Yates, 3rd, *A model for random sampling and estimation of relative protein abundance in shotgun proteomics*. Anal Chem, 2004. **76**(14): p. 4193-201.
89. Smith, C.A., et al., *XCMS: processing mass spectrometry data for metabolite profiling using nonlinear peak alignment, matching, and identification*. Anal Chem, 2006. **78**(3): p. 779-87.
90. Stein, S.E., *An integrated method for spectrum extraction and compound identification from gas chromatography/mass spectrometry data*. Journal of the American Society for Mass Spectrometry, 1999. **10**(8): p. 770-781.
91. Ma, L., et al., *The human TAZ gene complements mitochondrial dysfunction in the yeast taz1Delta mutant. Implications for Barth syndrome*. J Biol Chem, 2004. **279**(43): p. 44394-9.

92. Claypool, S.M., et al., *The cardiolipin transacylase, tafazzin, associates with two distinct respiratory components providing insight into Barth syndrome*. Mol Biol Cell, 2008. **19**(12): p. 5143-55.
93. Brandner, K., et al., *Taz1, an outer mitochondrial membrane protein, affects stability and assembly of inner membrane protein complexes: implications for Barth Syndrome*. Mol Biol Cell, 2005. **16**(11): p. 5202-14.
94. Zhang, M., E. Mileykovskaya, and W. Dowhan, *Gluing the respiratory chain together. Cardiolipin is required for supercomplex formation in the inner mitochondrial membrane*. J Biol Chem, 2002. **277**(46): p. 43553-6.
95. Nalecz, K.A., et al., *The monocarboxylate carrier from bovine heart mitochondria: partial purification and its substrate-transporting properties in a reconstituted system*. Biochim Biophys Acta, 1986. **851**(1): p. 29-37.
96. Kashfi, K., et al., *Membrane microenvironment regulation of carnitine palmitoyltransferases I and II*. Biochem Soc Trans, 2011. **39**(3): p. 833-7.
97. Nouws, J., et al., *Acyl-CoA dehydrogenase 9 is required for the biogenesis of oxidative phosphorylation complex I*. Cell Metab. **12**(3): p. 283-94.
98. Gerards, M., et al., *Riboflavin-responsive oxidative phosphorylation complex I deficiency caused by defective ACAD9: new function for an old gene*. Brain. **134**(Pt 1): p. 210-9.
99. Lee, I. and C.K. Suzuki, *Functional mechanics of the ATP-dependent Lon protease-lessons from endogenous protein and synthetic peptide substrates*. Biochim Biophys Acta, 2008. **1784**(5): p. 727-35.
100. Cade, W.T., et al., *Substrate metabolism during basal and hyperinsulinemic conditions in adolescents and young-adults with Barth syndrome*. J Inherit Metab Dis, 2012.
101. Wanders, R.J., et al., *Bicarbonate and the pathway of glutamate oxidation in isolated rat-liver mitochondria*. Eur J Biochem, 1983. **133**(1): p. 245-54.
102. Gebert, N., et al., *Mitochondrial cardiolipin involved in outer-membrane protein biogenesis: implications for Barth syndrome*. Curr Biol, 2009. **19**(24): p. 2133-9.

103. Malhotra, A., et al., *Formation of molecular species of mitochondrial cardiolipin. 1. A novel transacylation mechanism to shuttle fatty acids between sn-1 and sn-2 positions of multiple phospholipid species*. *Biochim Biophys Acta*, 2009. **1791**(4): p. 314-20.